Title: Bivalent mRNA booster encoding virus-like particles elicits potent polyclass receptor-binding domain antibodies in pre-vaccinated mice

Authors: Chengcheng Fan[1,7], Alexander A. Cohen[1,7], Kim-Marie A. Dam[2,7], Annie V. Rorick[1,3], Ange-Célia I. Priso Fils[1], Zhi Yang[1,4], Priyanthi N. P. Gnanapragasam[1], Luisa N. Segovia[1], Kathryn E. Huey-Tubman[1], Woohyun J. Moon[5], Paulo J.C. Lin[5], Pamela J. Bjorkman[1*], Magnus A. G. Hoffmann[2,6*]

Affiliations:

[1]Division of Biology and Biological Engineering, California Institute of Technology, Pasadena, CA 91125, USA

[2]Gladstone Institutes, San Francisco, CA 94158, USA

[3]Present address: Department of Biochemistry, University of Washington, Seattle, WA 98109, USA

[4]Present address: Department of Molecular and Cell Biology, University of California, Berkeley, Berkeley, CA 94720, USA

[5]Acuitas Therapeutics, Vancouver, BC, V6T 1Z3, CANADA

[6]Department of Medicine, University of California, San Francisco, CA 94143, USA

[7]These authors contributed equally

[*]To whom correspondence should be addressed: Email: bjorkman@caltech.edu, magnus.hoffmann@gladstone.ucsf.edu

Abstract

mRNA vaccines emerged as a leading vaccine technology during the COVID-19 pandemic. However, their sustained protective efficacies were limited by relatively short-lived antibody responses and the emergence of SARS-CoV-2 variants, necessitating frequent and variant-updated boosters. We recently developed the ESCRT- and ALIX-binding region (EABR) mRNA vaccine platform, which encodes engineered immunogens that induce budding of enveloped virus-like particles (eVLPs) from the plasma membrane, thereby resulting in presentation of immunogens on cell surfaces and eVLPs. Prior studies showed that spike (S)-EABR mRNA-LNP immunizations elicited enhanced neutralizing antibody responses against ancestral and variant SARS-CoV-2 compared with conventional S mRNA-LNP in naïve mice, but the effectiveness of S-EABR mRNA-LNP boosters in the context of pre-existing immunity has not been investigated. Here, we evaluated monovalent Wuhan-Hu-1 (Wu1) and bivalent (Wu1/BA.5) S-EABR mRNA-LNP boosters in mice pre-vaccinated with conventional Wu1 S mRNA-LNP. Compared to conventional S mRNA-LNP boosters, the EABR approach enhanced monovalent and bivalent mRNA-LNP booster-induced neutralizing responses against Omicron subvariants BA.1, BA.5, BQ.1.1, and XBB.1, with bivalent S-EABR mRNA-LNP consistently eliciting the highest titers. Epitope mapping of polyclonal antisera by deep mutational scanning revealed that bivalent S-EABR mRNA-LNP boosted diverse "polyclass" anti-RBD responses, suggesting balanced targeting of multiple RBD epitope classes. In contrast, monovalent S, bivalent S, and monovalent S-EABR mRNA-LNP boosters elicited less diverse polyclonal serum responses primarily targeting immunodominant RBD epitopes. Cryo-EM structures demonstrated that bivalent mRNA

46 immunizations promote S heterotrimer formation, potentially enhancing bivalent S-EABR
47 mRNA-LNP booster-induced antibody breadth and polyclass epitope targeting by
48 activating cross-reactive B cells through intra-S crosslinking. These findings support the
49 future design of bivalent or multivalent S-EABR mRNA-LNP boosters as a promising
50 strategy to confer broader, and therefore potentially more durable, protection against
51 emerging SARS-CoV-2 variants and other rapidly evolving viruses.

52 **Introduction**

53 mRNA vaccines emerged as a leading platform for the rapid and scalable development
54 of effective vaccines during the COVID-19 pandemic[1]. Currently approved mRNA
55 vaccines encode the SARS-CoV-2 spike (S) trimer[2], the main target for neutralizing
56 antibodies (Abs) produced during natural infection[3]. S-encoding mRNAs formulated in
57 lipid nanoparticles (LNP) are taken up by cells, which promotes translation and cell
58 surface expression of S trimers to activate B cells[4]. Translation of mRNA-encoded S
59 protein within host cells also provides viral peptides for presentation on MHC class I
60 molecules, which are recognized by cytotoxic T cells[5,6].

61

62 Initial two-shot COVID-19 mRNA vaccination series became available in December 2020
63 after clinical studies demonstrated protection from severe disease after SARS-CoV-2
64 infection[7,8]. However, the durability of mRNA vaccine-induced immune protection was
65 limited by two factors. First, serum Ab levels contracted over several months[9]. Second,
66 SARS-CoV-2 variants acquired mutations in the S protein, which reduced their sensitivity
67 to vaccine-induced neutralizing Abs[10]. As a result, a third dose of the original mRNA
68 vaccine encoding the ancestral Wuhan-Hu-1 (Wu1) S protein was offered starting in fall
69 2021[11].

70

71 The emergence of the Omicron BA.1 variant in November 2021[12] sparked concern
72 because of its levels of substitution in S, especially in the receptor-binding domain (RBD),
73 resulting in effective evasion of Ab-mediated immunity[13,14] and increased rates of
74 symptomatic infections in previously vaccinated individuals[15,16]. Although undetectable

after the initial mRNA vaccine series, a third dose of the original mRNA vaccine elicited neutralizing Abs against BA.1, but BA.1 neutralizing titers were lower compared to titers against the ancestral Wu1 variant[17]. The subsequent emergence of Omicron subvariants such as BA.5, BQ.1.1, and XBB.1, which exhibited progressively reduced sensitivities to vaccine-induced neutralizing Abs[18], prompted the development of bivalent mRNA boosters, which included mRNAs encoding both the Wu1 and the BA.5 S proteins[19]. Preclinical and clinical studies found that bivalent boosters elicited modestly improved neutralizing Ab responses against Omicron subvariants compared to a fourth dose of the original monovalent vaccine[19-23], although some studies found no differences between monovalent and bivalent boosters following initial vaccination with the original Wu1 S-encoding mRNA vaccine[24,25]. Several studies[21,22,24,26-28] showed that the effectiveness of bivalent boosters was limited by immune imprinting, which occurs when prior exposure to an antigen shapes immunological responses to related antigens during subsequent exposures[29]. Instead of generating *de novo* Omicron-specific immune responses, bivalent boosters primarily activated pre-existing cross-reactive memory B cells from previous vaccinations and/or infections[26-28], leading to lower neutralizing activity against Omicron subvariants compared to the ancestral variant[21,22,24].

Continued development of updated boosters in response to emerging variants was slowed by the need for additional clinical testing, regulatory approvals, and adjustments to the manufacturing process. As a result, bivalent boosters became available in fall 2022, almost one year after the emergence of Omicron[30]. These challenges highlight the urgent need for innovative vaccine strategies that achieve more lasting immune protection

98 against rapidly-evolving viruses such as SARS-CoV-2, thereby reducing the need for
99 frequent and updated boosters.
100
101 We recently developed the ESCRT- and ALIX-binding region (EABR) mRNA vaccine
102 platform that combines features of mRNA and protein nanoparticle (NP) vaccines through
103 delivery of mRNA-encoded self-assembling enveloped virus-like particles (eVLPs)[31].
104 eVLP assembly is achieved by fusing a short EABR sequence to the cytoplasmic tail of
105 viral surface proteins, which recruits proteins from the Endosomal Sorting Complex
106 Required for Transport (ESCRT) pathway. Thus, EABR mRNA vaccines promote dual
107 presentation of S trimers on cell surfaces and eVLPs that bud from the plasma membrane.
108 Immunizations in mice showed that an EABR mRNA vaccine encoding a Wu1 SARS-
109 CoV-2 S elicited superior neutralizing Ab potency and breadth against ancestral and
110 Omicron SARS-CoV-2 variants compared to conventional mRNA and protein NP
111 vaccines[31]. Similar to conventional mRNA vaccines, the EABR mRNA vaccine also
112 induced potent T cell responses, consistent with the presence of S-specific cytotoxic T
113 cells[31]. These findings suggest that the EABR mRNA vaccine approach has the potential
114 to enhance monovalent or bivalent booster-induced Ab responses against Omicron
115 subvariants in the context of pre-existing immunity induced by prior vaccination, infection,
116 or both.
117
118 Here, we evaluated the ability of EABR mRNA boost immunogens to elicit potent and
119 broad humoral immune responses against SARS-CoV-2 variants in pre-vaccinated mice.
120 We demonstrate that the EABR mRNA vaccine approach improves monovalent and

121 bivalent booster-mediated neutralizing Ab responses against Omicron subvariants
122 compared to conventional mRNA boosters. Epitope mapping of polyclonal antisera further
123 showed that a bivalent EABR mRNA booster elicited a more diversified anti-RBD IgG
124 response than other tested boosting immunogens. These findings support the use of the
125 EABR mRNA vaccine platform for the design of effective boosters that could confer more
126 lasting protection against SARS-CoV-2 variants and potentially other rapidly-evolving
127 viruses. In addition, our work provides structural evidence that bivalent mRNA
128 immunizations promote heterotrimer formation, which could enhance activation of cross-
129 reactive B cells through intra-S crosslinking. These insights inform the future design of
130 bivalent or multivalent COVID-19 boosters and highlight the need for further investigation
131 into potentially beneficial effects of S heterotrimer formation on vaccine-induced immune
132 responses against trimeric viral Ss.
133
134 **Results**
135 To expand upon our previous characterizations of a monovalent SARS-CoV-2 S-EABR
136 mRNA vaccine[31], we evaluated the potential of the EABR mRNA vaccine approach for
137 monovalent and bivalent SARS-CoV-2 immunizations in pre-vaccinated mice. Four
138 cohorts of 10 BALB/c mice each initially received prime-boost intramuscular (IM)
139 vaccinations on days 0 and 28 with 2 μg of a conventional mRNA vaccine encoding the
140 ancestral S protein from the Wu1 variant, similar to the immunogens used in initially
141 approved COVID-19 mRNA vaccines (Wu1 S mRNA-LNP) (Fig. 1A-C). To simulate the
142 timing of the third available COVID-19 mRNA vaccine dose in humans, booster
143 immunizations were administered on day 230, nearly 7 months after the primary

144 vaccination series, with each cohort receiving a different boost immunogen (Fig. 1A-C).
145 Consistent with the COVID-19 booster that became available in fall 2021[11], cohort 1
146 received a third dose of 2 μg Wu1 S mRNA-LNP (Fig. 1B-C). To evaluate whether
147 formation of mRNA-encoded S-EABR eVLPs enhances booster immunogenicity in pre-
148 vaccinated mice, cohort 2 received 2 μg Wu1 S-EABR mRNA-LNP (Fig. 1B-C). Cohort 3
149 received a bivalent Wu1/BA.5 S mRNA-LNP booster (1 μg Wu1 S mRNA-LNP combined
150 with 1 μg BA.5 S mRNA-LNP), which resembled the COVID-19 booster that became
151 available in fall 2022[30] (Fig. 1B-C). Lastly, cohort 4 received a bivalent Wu1/BA.5 S-EABR
152 mRNA-LNP booster to promote the formation of eVLPs that co-display Wu1 and BA.5 S
153 trimers (Fig. 1B-C). The Wu1 and BA.5 S-EABR constructs were designed as previously
154 described by fusing an endocytosis-preventing motif (EPM), a short Gly-Ser linker, and
155 an EABR sequence to the end of the cytoplasmic domain of Wu1 and BA.5 S trimers[31]
156 (Fig. S1A). The Wu1 and BA.5 S-EABR constructs induced similar levels of eVLP budding
157 in transiently transfected HEK293T cells (Fig. S1B).
158
159 Serum binding Ab responses were measured by enzyme-linked immunosorbent assay
160 (ELISA) four and 18 weeks after the primary vaccination series (days 56 and 154) and
161 two weeks after the booster immunizations (day 244). As previously observed, the initial
162 Wu1 S mRNA-LNP vaccinations elicited high binding Ab titers against soluble Wu1 S-6P
163 trimers[32], and as expected, these titers were similar for all cohorts on day 56 (Fig. 1D).
164 Robust binding Ab responses were also detected for all cohorts against Omicron BA.5,
165 BQ.1.1, and XBB.1 S-6P trimers on day 56 (Fig. 1E-G). On day 154, binding Ab levels
166 against all variants dropped slightly, which was consistent between cohorts (Fig. 1D-G).

167 On day 244, all boost immunogens increased binding Ab titers against Wu1, BA.5,
168 BQ.1.1, and XBB.1 S-6P trimers compared to titers measured on days 56 and 154, but
169 no differences were observed between cohorts for all timepoints (Fig. 1D-G).
170
171 **Bivalent S-EABR mRNA-LNP booster elicits potent Ab responses targeting**
172 **Omicron RBDs.**
173 We next evaluated the impact of the different boost immunizations on Ab responses
174 against the RBD, the primary target of neutralizing Abs[3]. The initial Wu1 S mRNA-LNP
175 prime-boost vaccinations elicited robust and similar Ab responses against the Wu1 RBD
176 for all cohorts on day 56 (Fig. 2A). The BA.5, BQ.1.1, and XBB.1 variants harbor multiple
177 RBD substitutions, particularly within the class 1 and 2 epitopes at the tip of the RBD[33]
178 (Fig. S2), promoting effective escape from neutralizing Abs[18]. Compared to Wu1 RBD
179 binding, Ab binding titers were weaker against the BA.5, BQ.1.1, and XBB.1 RBDs on day
180 56 (Fig. 2B-D). The robust Ab binding against the BA.5, BQ.1.1, and XBB.1 S trimers (Fig.
181 1E-G) in the absence of strong RBD responses was at least in part driven by potent
182 responses against the S2 region of S (Fig. S3), which is relatively conserved in SARS-
183 CoV-2 variants[34] (Fig. S2). Similar to binding titers against S-6P trimers (Fig. 1D-G), Wu1,
184 BA.5, BQ.1.1, and XBB.1 RBD binding slightly dropped on day 154 without statistically
185 significant differences between cohorts (Fig. 2A-D). The booster immunizations increased
186 Wu1 RBD binding on day 244 compared to day 56 and 154 levels, but no differences
187 were detected between the four boosting immunogens (Fig. 2A). In contrast, the bivalent
188 Wu1/BA.5 S-EABR mRNA-LNP booster elicited the highest BA.5, BQ.1.1, and XBB.1
189 RBD responses on day 244 (Fig. 2B-D), which were significantly higher than Wu1 S

190 mRNA-LNP booster-induced responses against BQ.1.1 RBD (p = 0.0499) (Fig. 2C) and
191 narrowly failed to reach statistical significance compared to Wu1 S mRNA-LNP booster-
192 induced responses against BA.5 RBD (p = 0.07) (Fig. 2B). Compared to baseline titers
193 measured prior to boost immunizations on day 154, the bivalent Wu1/BA.5 S-EABR
194 mRNA-LNP immunization elicited significantly larger increases in BA.5 RBD binding than
195 the monovalent Wu1 S mRNA-LNP (p = 0.02) and the bivalent Wu1/BA.5 S mRNA-LNP
196 boosters (p = 0.01) (Fig. 2B), as well as significantly larger increases in BQ.1.1 RBD
197 binding than the Wu1 S mRNA-LNP booster (p = 0.002) (Fig. 2C). While overall titers
198 were similar on day 244, the monovalent Wu1 S-EABR mRNA-LNP booster consistently
199 induced larger increases in Ab binding to the BA.5, BQ.1.1, and XBB.1 RBDs than the
200 monovalent Wu1 S mRNA-LNP booster (Fig. 2B-D), although these differences failed to
201 reach statistical significance. The monovalent Wu1 and bivalent Wu1/BA.5 S mRNA-LNP
202 boosters elicited similar binding titers against the BA.5 and XBB.1 RBDs (Fig. 2B and D),
203 but the bivalent booster induced slightly higher responses and a larger increase
204 compared to day 154 titers against BQ.1.1 RBD (not statistically significant) (Fig. 2C).
205 Overall, these results demonstrate that booster immunizations with the bivalent Wu1/BA.5
206 S-EABR mRNA-LNP elicited the highest Ab responses against Omicron RBDs in pre-
207 vaccinated mice. Notably, post-boost Ab binding against Omicron RBDs remained lower
208 than binding titers against Wu1 RBD in all cohorts, suggesting that booster responses
209 were affected by immune imprinting induced by the primary vaccination series.
210
211

212 **Bivalent S-EABR mRNA-LNP booster elicits higher neutralizing responses against**
213 **Omicron variants.**

214 The ability of boost immunogens to elicit neutralizing Ab responses in pre-vaccinated mice
215 was evaluated by in vitro pseudovirus neutralization assays[35,36]. The primary vaccination
216 series with Wu1 S mRNA-LNP elicited potent and consistent autologous geometric mean
217 neutralizing titers as assessed by half-maximal serum inhibitory dilution (ID_{50}) values
218 against Wu1 pseudovirus in all cohorts on day 56 (Fig. 3A; Table S1). Neutralizing activity
219 was >100-fold lower against the BA.5 variant and undetectable in most animals against
220 the BQ.1.1 and XBB.1 variants on day 56 for all cohorts (Fig. 3B-D; Table S1). On day
221 154, neutralizing titers against the Wu1 and BA.5 variants were consistent in all cohorts
222 and slightly lower compared to day 56 titers (Fig. 3A-B; Table S1). Neutralizing activity
223 against the BQ.1.1 and XBB.1 variants was undetectable in all but one animal on day 154
224 (Fig. 3C-D; Table S1). Booster immunizations on day 230 increased autologous
225 neutralizing titers against Wu1 pseudovirus on day 244 compared to day 154 in all cohorts
226 (Fig. 3A; Table S1). Monovalent Wu1 S mRNA-LNP and S-EABR mRNA-LNP
227 immunizations elicited the smallest and largest increases in Wu1 neutralization (4.2-fold
228 versus 6.6-fold), respectively. All boost immunogens elicited increased BA.5 neutralizing
229 activity on day 244 compared to day 56 and 154 titers (Fig. 3B; Table S1). Boosting with
230 monovalent Wu1 S-EABR mRNA-LNP induced 4.8-fold higher BA.5 neutralizing titers
231 than a third Wu1 S mRNA-LNP immunization, but this difference did not reach statistical
232 significance. Using the respective day 154 titers as baseline, the Wu1 S-EABR mRNA-
233 LNP booster induced a 23.8-fold increase in BA.5 neutralization on day 244 compared to
234 only a 6.3-fold increase detected after boosting with Wu1 S mRNA-LNP (not statistically

235 significant) (Fig. 3B; Table S1). Compared to day 56 baseline titers, the Wu1 S-EABR
236 mRNA-LNP booster induced a significantly higher increase in BA.5 neutralization on day
237 244 than the conventional Wu1 S mRNA-LNP booster (16.2-fold versus 3.1-fold; p =
238 0.048) (Fig. S4; Table S1). The Wu1 S-EABR mRNA-LNP booster also elicited 3.4-fold
239 higher neutralizing responses than the Wu1 S mRNA-LNP booster against the Omicron
240 BA.1 variant on day 244 (p = 0.03) (Fig. S5). Based on day 154 titers, boosting with
241 monovalent Wu1 S-EABR mRNA-LNP induced significantly higher increases in BA.1
242 neutralization compared to monovalent Wu1 S mRNA-LNP (8.8-fold versus 2.5-fold; p =
243 0.009) (Fig. S5). Interestingly, the monovalent Wu1 S-EABR mRNA-LNP and the bivalent
244 Wu1/BA.5 S mRNA-LNP boosters elicited similar BA.5 neutralizing responses on day 244
245 (Fig. 3B; Table S1), suggesting that the EABR mRNA vaccine approach might reduce the
246 need for updating boost immunogens to achieve robust Ab responses against emerging
247 SARS-CoV-2 variants. The highest BA.5 neutralizing titers were elicited by the bivalent
248 Wu1/BA.5 S-EABR mRNA-LNP booster, which were 12.3-fold higher than titers induced
249 by the monovalent Wu1 S mRNA-LNP booster (p = 0.02) and 2.4-fold higher than titers
250 induced by the bivalent Wu1/BA.5 S mRNA-LNP booster (not statistically significant).
251 Based on titers measured on day 154, the Wu1/BA.5 S-EABR mRNA-LNP booster
252 induced a 67-fold increase in BA.5 neutralization, which was significantly higher than the
253 increase elicited by boosting with monovalent Wu1 S mRNA-LNP (p = 0.003).
254
255 While the BA.5 neutralizing activity induced by the monovalent Wu1 S and S-EABR
256 mRNA-LNP boosters can likely be attributed to cross-neutralizing Abs that neutralize both
257 the Wu1 and BA.5 variants, it is possible that the bivalent Wu1/BA.5 S and S-EABR

258 mRNA-LNP boosters also elicited *de novo* strain-specific Abs that neutralize BA.5 but not
259 Wu1. Day 244 serum samples from mice that received bivalent Wu1/BA.5 S or S-EABR
260 mRNA-LNP boosters were depleted of Abs that bind to Wu1 RBD. Sera were passaged
261 over a column presenting either a mock protein (HIV-1 gp120) as a control or the Wu1
262 RBD to remove cross-neutralizing anti-RBD Abs while retaining BA.5 RBD-specific Abs.
263 Following depletions, residual neutralization activity was measured against the BA.5
264 variant. Interestingly, Wu1 RBD depletion resulted in 17- and 36-fold lower geometric
265 mean neutralizing titers compared to mock depletion for the bivalent Wu1/BA.5 S and S-
266 EABR mRNA-LNP boosters, respectively (Fig. S6). In both cohorts, BA.5 neutralizing
267 titers in all but two mice dropped below ID_{50} values of 1:120 following Wu1 RBD depletion,
268 consistent with the neutralizing activity in these samples being primarily driven by cross-
269 neutralizing Abs targeting the RBD induced by the primary vaccination series. The potent
270 residual neutralizing activity observed in two mice in each cohort after Wu1 RBD depletion
271 implies either the presence of boost-induced *de novo* BA.5-specific RBD Abs or
272 neutralizing non-RBD Abs that target another region of S, e.g., the N-terminal domain[37]
273 or S2[34].
274
275 Booster immunizations had less pronounced effects on neutralization activity against the
276 BQ.1.1 and XBB.1 variants. Against BQ.1.1 pseudovirus, the bivalent Wu1/BA.5 S-EABR
277 mRNA-LNP booster elicited the most potent neutralizing activity on day 244, which was
278 significantly higher than responses induced by a third immunization with the monovalent
279 Wu1 S mRNA-LNP booster ($p = 0.0495$) (Fig. 3C; Table S1). The monovalent Wu1 S-
280 EABR mRNA-LNP and bivalent Wu1/BA.5 S mRNA-LNP boosters elicited 1.8- and 2.5-

281 fold higher BQ.1.1 titers than the monovalent Wu1 S mRNA-LNP booster, respectively,
282 the latter of which narrowly failed to reach statistical significance ($p = 0.07$). Based on day
283 154 BQ.1.1 neutralizing titers, the monovalent Wu1 S mRNA-LNP and bivalent Wu1/BA.5
284 S-EABR mRNA-LNP boosters induced the smallest and largest increases in neutralizing
285 activity on day 244, respectively (1.4-fold versus 4.7-fold; $p = 0.0495$). The monovalent
286 Wu1 S-EABR mRNA-LNP and bivalent Wu1/BA.5 S mRNA-LNP boosters elicited 2.4-
287 and 3.4-fold increases in neutralizing BQ.1.1 titers, respectively. Notably, day 244
288 neutralizing titers against BQ.1.1 were substantially lower than BA.5 neutralizing titers for
289 all boost immunogens (Fig. 3B-C; Table S1), consistent with previous reports[18,38]. Notably,
290 Ab binding responses against the BA.5 and BQ.1.1 RBDs were similar (Fig. 2B-C),
291 implying that RBD binding responses are not always predictive of neutralizing activity
292 against Omicron subvariants.
293
294 Neutralizing responses against the XBB.1 variant were slightly lower than titers against
295 BQ.1.1 pseudovirus (Fig. 3D; Table S1). Once again, the bivalent Wu1/BA.5 S-EABR
296 mRNA-LNP booster elicited the highest XBB.1 neutralizing titers, which were 2.1-fold
297 higher than titers induced by the monovalent Wu1 S mRNA-LNP booster (not statistically
298 significant). Based on day 154 titers, the monovalent Wu1 and bivalent Wu1/BA.5 S-
299 EABR mRNA-LNP boosters increased XBB.1 neutralization by 2.5- and 3.2-fold,
300 respectively, while conventional monovalent and bivalent S mRNA-LNP boosters only
301 induced 1.5- and 2.2-fold increases, respectively.
302

303 Notable differences were also observed in the number of mice in each cohort that reached
304 robust neutralizing titers (defined as ID_{50}s exceeding 1:100) against Omicron subvariants
305 following booster immunizations, titers that are likely important for the prevention of
306 symptomatic infections[39]. The primary vaccination series with Wu1 S mRNA-LNP elicited
307 robust neutralizing titers against the Wu1 variant in all mice on day 56 (Fig. 3F). However,
308 the initial Wu1 S mRNA-LNP vaccinations elicited robust titers in only 6 to 8, 1 to 3, and
309 0 to 2 of 10 mice against the BA.5, BQ.1.1, and XBB.1 variants on day 56, respectively.
310 On day 154, ID_{50}s over 1:100 were measured for 3 to 5 mice in each cohort against BA.5,
311 but for none of the animals against BQ.1.1 and XBB.1. While a third immunization with
312 Wu1 S mRNA-LNP induced robust titers against BA.5 in only 8 of 10 mice on day 244,
313 the monovalent Wu1 S-EABR mRNA-LNP booster induced robust titers against BA.5 in
314 all 10 mice, including the 4 mice that did not have detectable BA.5 neutralizing activity on
315 day 56 (Fig. 3F). As expected, robust neutralizing titers against the BA.5 variant were also
316 observed in all mice that received the bivalent Wu1/BA.5 S or S-EABR mRNA-LNP
317 boosters. Against the BQ.1.1 and XBB.1 variants, a third immunization with Wu1 S
318 mRNA-LNP induced robust neutralizing titers in only 2 and 3 mice, respectively (Fig. 3F).
319 In comparison, the bivalent Wu1/BA.5 S-EABR mRNA-LNP booster induced ID_{50}s over
320 1:100 in 7 and 6 mice against the BQ.1.1 and XBB.1 variants, respectively.
321
322 Overall, these results demonstrate that the EABR mRNA vaccine approach improves the
323 neutralizing activity against Omicron subvariants induced by monovalent and bivalent
324 boost immunogens in pre-vaccinated mice.
325

326 **Bivalent S-EABR mRNA-LNP booster induces polyclass Ab responses.**

327 Several distinct Ab-binding epitopes have been defined on RBDs, including the variable
328 class 1 and 2 RBD epitopes and the more conserved class 3, 4, 1/4, and 5 RBD
329 epitopes[33,40,41] (Fig. S2). We determined which RBD epitopes were targeted by booster-
330 induced Abs in pre-vaccinated mice using deep mutational scanning (DMS) of yeast
331 display libraries derived from Wu1[42] and XBB.1.5 RBDs[43]. In previous studies, we showed
332 that equimolar mixtures of monoclonal Abs targeting distinct RBD epitopes produced less
333 pronounced DMS escape peaks, which we defined as a polyclass Ab response[44]. This
334 suggests that polyclonal serum that includes roughly equal distributions of Abs targeting
335 multiple classes of RBD epitopes would exhibit relatively flat DMS profiles, while more
336 defined DMS escape peaks would be observed for less diverse polyclonal serum
337 responses containing Abs that primarily target particular RBD epitopes[44]. For this study,
338 we used DMS escape fractions to define polyclass responses. Escape fractions for each
339 RBD mutation range from 0 (no cells with this mutation are sorted into the serum Ab
340 escape bin) to 1 (all cells with this mutation are sorted into the serum Ab escape bin)[45].
341 Total escape peaks represent the sum of escape fractions for all mutations at a specific
342 site[45]. DMS profiles with total escape peaks below 0.5 at all sites were classified as
343 polyclass responses. In contrast, DMS profiles with total escape peaks of 0.5-1, 1-2, or
344 above 2 at one or more sites were classified as weak, moderate, or strong escape profiles,
345 respectively, indicating weak, moderate, or strong targeting of particular RBD epitopes
346 (Table S2). DMS was performed for 6 serum samples for each cohort, which were
347 selected based on XBB.1 neutralization activity (1st, 2nd, 3rd, 5th, 6th, and 10th best

348 neutralizer from each cohort). For the Wu1 RBD library, only 5 DMS profiles were obtained
349 due to poor sequencing quality for one sample in each cohort.
350
351 Against the Wu1 RBD library, immunizations with the monovalent Wu1 S and S-EABR
352 mRNA-LNP boosters or the bivalent Wu1/BA.5 S mRNA-LNP booster resulted in DMS
353 profiles consistent with moderate targeting of the variable class 2 epitope primarily
354 inducing escape at RBD residue 484 (Fig. 4A-B). The bivalent Wu1/BA.5 S mRNA-LNP
355 booster also elicited weak to moderate responses that mapped to the variable class 1
356 and class 3 RBD epitopes. In contrast, the bivalent Wu1/BA.5 S-EABR mRNA-LNP
357 booster DMS profiles were consistent with polyclass Ab induction, suggesting a more
358 diverse response targeting multiple RBD epitopes (Fig. 4A-B). Notably, samples from 4
359 out of 5 mice in this cohort exhibited polyclass DMS profiles, whereas moderate to strong
360 escape fractions for class 1, 2, or 3 epitopes were observed in 3-4 mice in each of the
361 other cohorts (Fig. S7; Table S2).
362
363 As expected, no class 1 and 2 DMS profiles were observed against the XBB.1.5 RBD
364 library[43] since these epitopes are highly substituted in Omicron subvariants (Fig. S2). All
365 booster immunizations induced strong class 5 escape peaks targeting RBD residues 352,
366 357, 396, and 468 (Fig. 4C-D). Importantly, the bivalent Wu1/BA.5 S-EABR mRNA-LNP
367 booster induced a less pronounced overall class 5 profile than the other boost
368 immunogens, which was primarily driven by a strong class 5 response observed in a
369 single animal in this cohort (Fig. S8; Table S2). The other mice that received the bivalent
370 Wu1/BA.5 S-EABR mRNA-LNP booster exhibited polyclass or weak to moderate

371 responses against class 4 and 5 epitopes. In contrast, strong class 5 profiles were
372 detected in 4-5 mice in cohorts that received the monovalent Wu1 S or S-EABR mRNA-
373 LNP boosters or the bivalent Wu1/BA.5 S mRNA-LNP booster (Fig. S8; Table S2).
374 Overall, these results suggest that the bivalent Wu1/BA.5 S-EABR mRNA-LNP booster
375 induced a more diversified polyclass Ab response that likely contributed to the higher
376 neutralizing activity observed against Omicron subvariants, which could result in more
377 effective recognition of future variants.
378
379 **Co-expression of Wu1 and BA.5 S results in heterotrimer formation.**
380 The results from this and previous studies[19-22] demonstrated that bivalent booster
381 immunizations improve the potency and breadth of Ab responses against Omicron
382 subvariants compared to monovalent boosters. Serum depletion assays also showed that
383 the BA.5 neutralizing activity elicited by the bivalent Wu1/BA.5 S and S-EABR mRNA-
384 LNP boosters was primarily driven by cross-reactive Abs that bind to the Wu1 and BA.5
385 RBDs (Fig. S6). Preferential activation of cross-reactive B cells could be achieved through
386 co-display of Wu1 and BA.5 S trimers on the surface of a cell and/or an eVLP (Fig. 1C),
387 which could result in inter-S crosslinking between cross-reactive B cell receptors (BCRs)
388 and neighboring homotrimeric Wu1 and BA.5 S trimers (Fig. S9). As an additional
389 mechanism for bivalent booster-induced activation of cross-reactive B cells, we
390 hypothesized that co-expression of ancestral Wu1 and Omicron S in the same cell could
391 result in the formation of S heterotrimers consisting of Wu1 and Omicron S protomers and
392 could promote intra-S crosslinking, i.e., simultaneous binding of cross-reactive BCRs to
393 two neighboring RBDs within the same S trimer (Fig. S9). We previously postulated that

394 intra-S crosslinking is possible for several anti-RBD IgGs based on modeling of intact IgG
395 coordinates into single-particle cryo-electron microcopy (cryo-EM) structures of fragment
396 antigen-binding (Fab)-S complexes[33,40], and intra-S crosslinking was observed in EM
397 studies of IgG-S trimer complexes[46]. However, it is currently unknown whether co-
398 expression of Wu1 and Omicron Ss induces heterotrimerization, and if so, whether
399 heterotrimer formation affects the overall structure of the S ectodomain and influences
400 bivalent booster-induced immune responses.
401
402 To investigate whether S heterotrimers could form with different S protomers, we
403 designed 6P versions[32] of Wu1/BA.1 and Wu1/BA.1/Delta soluble heterotrimer Ss (HT2
404 and HT3, respectively) by co-transfection with specific C-terminally-tagged constructs.
405 HT2 was generated by co-transfecting StrepII-tagged Wu1 S and His-tagged BA.1 S,
406 while HT3 was generated using StrepII-tagged Wu1 S, His-tagged BA.1 S, and D7324[47]-
407 tagged Delta S (Fig. 5A). Each heterotrimer was subsequently purified using sequential
408 affinity purification specific to each tag, confirming the inclusion of distinct protomers in
409 the purified heterotrimers (Fig. 5A).
410
411 HT2 and HT3 S proteins were then evaluated using single-particle cryo-electron
412 microscopy (cryo-EM) to determine whether heterotrimeric Ss resembling their
413 homotrimeric counterparts were formed. To ensure that C-terminal tags did not disrupt
414 the formation of trimers, we included the following controls: (1) three homotrimers with
415 single tags (StrepII-tagged Wu1 S, His-tagged BA.1 S, and D7324-tagged Delta S), and
416 (2) a homotrimer comprised of His- and StrepII-tagged protomers (Wu1-His/Wu1-StrepII).

417 Single-particle cryo-EM analysis confirmed that all control S proteins formed trimers,
418 indicating that C-terminal tags did not disrupt trimerization (Fig. S10). Because most of
419 the EM constructions for homotrimeric S controls exhibited preferred orientations, we
420 determined overall conformational states (Fig. 5) for the control structures but did not fit
421 atomic models. Structural analysis also revealed trimerized HT2 and HT3 Ss (Fig. 5B-C,
422 Fig. S10). Although atomic models could not be built for the HT2 and HT3 trimer
423 reconstructions because the identities of individual protomers (Wu1 or BA.1 for HT2, and
424 Wu1, BA.1, or Delta for HT3) could not be conclusively determined at relatively low
425 resolution, the EM densities of S heterotrimers and control homotrimers showed no major
426 conformational differences in domain organization (Fig. 5B-C, Fig. S10). As previously
427 seen in SARS-CoV-2 S trimer structures[48,49], we observed two trimer populations in all
428 datasets—one with all three RBDs in the 'down' conformation and one with a single RBD
429 in an 'up' conformation (Fig. 5D). These data demonstrate heterotrimeric S formation for
430 soluble forms of SARS-CoV-2 S proteins. This result suggests that the bivalent S or S-
431 EABR mRNA-LNP boost immunogens likely induce heterotrimerization, which could
432 promote activation of cross-reactive B cells through intra-S cross-linking, a potential
433 mechanism warranting further investigation.
434

435 **Discussion**

436 The EABR mRNA vaccine platform delivers mRNA encoding engineered immunogens
437 that induce budding of enveloped virus-like particles (eVLPs) from the plasma membrane
438 to promote presentation of immunogens on cell surfaces and eVLPs[31]. This approach
439 elicited superior neutralizing Ab responses in naïve mice compared to a conventional

440 mRNA vaccine against original and variant SARS-CoV-2[31]. However, the majority of the
441 human population has already mounted immune responses against SARS-CoV-2 through
442 prior vaccinations, natural infections, or a combination of both. Here, we demonstrate that
443 the EABR mRNA vaccine approach improves humoral immune responses elicited by
444 monovalent and bivalent mRNA-LNP booster immunizations against Omicron subvariants
445 in pre-vaccinated mice.
446
447 The possibility of receiving a third dose of the original COVID-19 mRNA vaccine in fall
448 2021[11] coincided with the emergence of the Omicron variants in November 2021[12]. These
449 variants had acquired many substitutions, especially in the RBD, which allowed efficient
450 evasion of Ab-mediated immunity[13,14] and rapid global spread. Similar to the effects of a
451 third vaccination in humans[17], a third immunization in pre-vaccinated mice with a
452 monovalent Wu1 S mRNA-LNP booster elicited modest neutralizing activity against the
453 early Omicron variants BA.1 and BA.5. However, addition of an EABR sequence[31] to the
454 boosting immunogen resulted in higher Ab neutralizing titers against BA.1 and BA.5,
455 suggesting that a monovalent Wu1 S-EABR booster could have promoted enhanced
456 protection against early Omicron variants. Importantly, the monovalent Wu1 S-EABR
457 mRNA-LNP booster elicited similar neutralizing responses against the BA.5, BQ.1.1, and
458 XBB.1 subvariants compared to the conventional bivalent S mRNA-LNP booster that
459 contained both Wu1 and BA.5 S immunogens.
460
461 While updating of mRNA vaccines can be done relatively quickly, the development,
462 clinical testing, approval, and large-scale manufacturing of a bivalent booster that

463 includes updated immunogens based on new circulating variants cannot be accomplished
464 fast enough to keep up with viral evolution during a global pandemic such as COVID-19.
465 Indeed, the Wu1/BA.5 bivalent booster became available in fall 2022, almost one year
466 after the emergence of Omicron variants[30]. The results reported here suggest that the
467 EABR mRNA vaccine approach presents a potential solution that could reduce the need
468 for frequent development of updated COVID-19 boosters and potentially future pandemic
469 viruses. Combined with our previous finding that an initial two-shot vaccination series with
470 a Wu1 S-EABR mRNA-LNP immunogen elicited substantially higher neutralizing activity
471 against Omicron variants than conventional Wu1 S mRNA-LNP immunizations in naïve
472 mice[31], our results demonstrate that the EABR mRNA vaccine approach has the potential
473 to induce more effective and lasting humoral immunity against emerging SARS-CoV-2
474 variants and represents a promising platform for future pandemic preparedness.
475
476 Clinical studies showed that the bivalent COVID-19 mRNA booster outperformed the
477 monovalent mRNA booster in terms of preventing symptomatic illness, hospitalizations,
478 and deaths when administered as a fourth dose in humans[30,50]. Consistent with other
479 studies[19-23], the bivalent conventional and EABR-based boosters evaluated in this study
480 elicited higher neutralizing responses against Omicron subvariants than their monovalent
481 counterparts in pre-vaccinated mice, although improvements were relatively modest.
482 However, the bivalent Wu1/BA.5 S-EABR mRNA-LNP booster consistently elicited the
483 highest RBD binding and neutralizing titers against all tested Omicron subvariants and
484 induced robust neutralizing responses in the highest number of animals against the
485 BQ.1.1 and XBB.1 variants that are particularly difficult to neutralize[18,38] These results

486 highlight that the EABR mRNA vaccine approach and the bivalent booster strategy work
487 synergistically to induce more effective humoral immune responses.
488
489 In addition to eliciting the most potent neutralizing responses against Omicron
490 subvariants, the bivalent Wu1/BA.5 S-EABR mRNA-LNP booster also induced distinct
491 DMS signatures compared to the other boost immunogens, consistent with differences in
492 epitope mapping of polyclonal anti-RBD Ab responses. While the monovalent Wu1 S and
493 S-EABR mRNA-LNP and the bivalent Wu1/BA.5 S mRNA-LNP boosters elicited
494 predominantly class 1 and class 2 responses against Wu1 RBD and strong class 5
495 responses against XBB.1.5 RBD, boost immunizations with bivalent Wu1/BA.5 S-EABR
496 mRNA-LNP elicited polyclass serum Ab responses against Wu1 RBD and mostly
497 polyclass or moderate polyclass class 4 and class 5 responses against XBB.1.5 RBD.
498 These results imply that combining the bivalent booster strategy with the EARB mRNA
499 vaccine approach elicited a more diversified Ab response, resulting in simultaneous and
500 balanced targeting of multiple RBD epitopes. A more diverse anti-RBD Ab response might
501 be desirable as viral immune evasion would require mutations in multiple sites, including
502 the more conserved class 4 and 5 RBD epitopes. As a potential mechanism for the more
503 frequent induction of polyclass-like Ab responses, we hypothesize that EABR eVLP
504 formation promotes close proximity of Wu1 and BA.5 S trimers on densely-coated eVLPs,
505 consistent with cryo-electron tomography imaging of purified eVLPs showing that the
506 density of S trimers was equivalent or higher than on SARS-CoV-2 virions (20-40 S
507 trimers on 40-60 nm diameter eVLPs)[31]. The high density of co-displayed Wu1 and BA.5
508 S trimers on eVLPs should facilitate inter-S crosslinking by B cell receptors that recognize

509 epitopes that are conserved between Wu1 and BA.5 S trimers, leading to preferential
510 activation of cross-reactive B cells. By comparison, conventional bivalent mRNA booster-
511 mediated co-expression of Wu1 and BA.5 S trimers could result in lower S trimer density
512 on cell surfaces that are crowded with endogenous membrane proteins, which could
513 prevent efficient inter-S crosslinking.
514
515 As an additional mechanism for bivalent booster-induced preferential activation of cross-
516 reactive B cells, we provide evidence that co-expression of ancestral and Omicron S
517 results in heterotrimer formation that could promote intra-S crosslinking, i.e.,
518 simultaneous binding of both Fabs of a cross-reactive BCR to neighboring RBDs within
519 the same S trimer. We previously postulated that intra-S crosslinking is possible for
520 several anti-RBD Abs that target various RBD epitopes based on modeling of intact IgG
521 structures onto cryo-EM structures of Fab-S complexes[33,40]. The conventional mRNA-
522 and the EABR mRNA-based bivalent boost immunogens should promote similar degrees
523 of heterotrimerization and intra-S crosslinking. While our RBD serum depletion assays
524 showed that both bivalent boosters primarily elicited cross-neutralizing Abs that bind to
525 the Wu1 and BA.5 RBDs, only the EABR mRNA-based bivalent booster induced
526 predominantly polyclass DMS signatures. Thus, it is possible that the diversification of the
527 anti-RBD Ab response observed for the bivalent EABR mRNA booster was primarily
528 driven by inter-S crosslinking possibly in conjunction with intra-S crosslinking. Future
529 studies are needed to investigate the impact of inter- and intra-S crosslinking on the
530 activation of cross-reactive B cells and to evaluate whether the EABR mRNA vaccine
531 approach can improve other types of bivalent and multivalent vaccines.

532 Although our results highlight the potential of the EABR mRNA vaccine approach in the
533 context of pre-existing immunity, we observed that monovalent and bivalent EABR mRNA
534 booster-induced humoral immune responses were still largely dictated by immunological
535 imprinting resulting from the initial vaccination series. Post-boost BA.5 neutralizing
536 responses were roughly an order of magnitude lower than Wu1 neutralization titers, even
537 for bivalent boosters that included BA.5 S immunogens. In addition, despite eliciting
538 consistent polyclass anti-RBD Ab responses, bivalent EABR mRNA booster-induced
539 neutralizing activity against the BQ.1.1 and XBB.1 variants dropped over 10-fold
540 compared to BA.5 neutralization. Notably, Ab binding responses to BQ.1.1 and XBB.1
541 RBDs were similar compared to BA.5 RBD binding for all boost immunogens. This
542 discrepancy between RBD binding responses and neutralization titers indicates that only
543 a relatively small fraction of binding Abs has neutralizing activity and/or the Abs still bind
544 to the BQ.1.1 and XBB.1 RBDs, but fail to effectively prevent interactions with ACE2 on
545 the surface of target cells. The initial two-shot COVID-19 mRNA vaccination series and
546 all booster immunizations elicited potent binding responses against the S2 region, which
547 is relatively conserved among SARS-CoV-2 variants[34]. Consistent with previous reports[51],
548 our depletion studies showed that anti-S2 Abs had little impact on virus neutralization,
549 which was instead predominantly driven by anti-RBD Abs. However, anti-S2 Abs could
550 still provide valuable immune protection against symptomatic Omicron infections through
551 Fc-mediated effector functions[52]. In addition, mRNA vaccines induce potent cytotoxic T
552 cell responses that cross-recognize Omicron variants[53] and reduce COVID-19 disease
553 severity[54].
554

555 Taken together, our results demonstrate that the EABR mRNA vaccine approach
556 improves monovalent and bivalent booster-mediated humoral immune responses against
557 Omicron subvariants in pre-vaccinated mice. DMS epitope mapping studies further
558 showed that the bivalent EABR mRNA booster elicited a more diversified anti-RBD Ab
559 response than all other tested boost immunogens. Our work also provides evidence that
560 bivalent mRNA booster immunizations promote heterotrimer formation, which could
561 activate cross-reactive B cells through intra-S crosslinking. Despite these advances,
562 future work is needed to develop booster strategies that overcome immunological
563 imprinting more effectively and confer lasting immunity against emerging variants.
564

565 **Limitations of the study**

566 Due to the substantial time required to conduct immunization studies in pre-vaccinated
567 mice, this proof-of-concept study to evaluate the potential of EABR-modified boosters in
568 the context of pre-existing immunity was performed using outdated SARS-CoV-2 variants.
569 Future studies are needed to assess EABR booster responses against currently
570 circulating variants. While the monovalent Wu1 S-EABR mRNA-LNP booster elicited
571 robust improvements in neutralization titers against BA.1 and BA.5 compared to the
572 conventional Wu1 S mRNA-LNP booster, consistent with previously reported results in
573 naïve mice[31], only modest and statistically non-significant increases were observed for
574 later Omicron variants, such as BQ.1.1 and XBB.1. Moreover, although the bivalent
575 Wu1/BA.5 S-EABR mRNA-LNP booster consistently induced the highest neutralizing
576 titers across all tested variants, these increases were statistically significant only relative
577 to the conventional monovalent Wu1 S mRNA-LNP and not the bivalent Wu1/BA.5 S

578 mRNA-LNP booster. Larger mouse cohorts could have increased the statistical power of
579 the study, such that the observed trends might have reached statistical significance.
580 Another factor contributing to the relatively modest improvements elicited by the
581 monovalent and bivalent EABR boosters against BQ.1.1 and XBB.1 was the generally
582 low levels of neutralizing responses observed against these variants. Although the low
583 neutralization activity against BQ.1.1 and XBB.1 was likely the result of immune imprinting
584 caused by the initial vaccination series, addition of more cohorts might have excluded the
585 possibility that the ancestral Wu1 S immunogen is more immunogenic than the Omicron
586 BA.5 S immunogen, e.g., three immunizations with monovalent BA.5 S or bivalent
587 Wu1/BA.5 S mRNA-LNP. However, this is unlikely since prior studies reported that
588 ancestral and Omicron S immunogens are similarly immunogenic[19,55,56]. Finally, it
589 remains unclear why the polyclonal RBD epitope–targeting response elicited by the
590 bivalent Wu1/BA.5 S-EABR mRNA-LNP booster translated into only modest gains in
591 neutralizing activity against Omicron variants. It is possible that a longer post-boost follow-
592 up period or an additional booster incorporating an XBB.1 S immunogen would have
593 revealed further maturation and expansion of these responses, and thereby additional
594 benefits of the bivalent EABR booster.
595

596 **Methods**

597 **Design of EABR constructs**

598 SARS-CoV-2 S-EABR constructs were designed as described[31]. The EABR domain
599 (residues 160-217) of the human CEP55 protein was fused to the C-terminus of the
600 SARS-CoV-2 S protein obtained from the Wu1 (GenBank: QTA38991.1) or BA.5

601 (GenBank: UPP14409.1) variants separated by a 4-residue $(Gly)_3Ser$ (GS) linker (Fig.
602 S1A). These constructs contained the native furin cleavage site, 2P stabilizing
603 mutations[57], and the C-terminal 21 residues were truncated to remove an endoplasmic
604 reticulum retention signal[58]. The D614G substitution[59], naturally present in BA.5, was
605 inserted into Wu1 S and S-EABR constructs. To prevent endocytosis and enhance the
606 cell surface expression of S-EABR constructs, an EPM (residues 243-290 of mouse
607 FcgRII-B1)[31,60] was inserted upstream of the 4-residue Gly-Ser linker and the EABR
608 domain as described[31] (Fig. S1A).
609

610 **In vitro transfection**

611 To verify that the designed constructs induce eVLP budding, HEK293T were transiently
612 transfected with DNA plasmids encoding Wu1 or BA.5 S-EABR using Fugene HD
613 (Promega). After 48 hours, transfected cell supernatants were harvested, and eVLPs
614 were purified by ultracentrifugation on a 20% sucrose cushion as described[31]. The purified
615 eVLP fractions were 3-fold serially diluted in 0.1 M $NaHCO_3$ pH 9.6, directly coated onto
616 Costar high binding 96-well plates (Corning), and eVLP-associated S protein levels were
617 quantified by ELISA. After 1 hour blocking in Tris-buffered saline with 0.1% TWEEN 20
618 (TBS-T) and 3% bovine serum albumin (BSA) (TBS-T/3% BSA) at room temperature, the
619 monoclonal anti-S2 Ab S2P6[61] was diluted to a concentration of 5 μg/mL in TBS-T/3%
620 BSA and added to plates for 1 hour at room temperature. After washing with TBS-T, HRP-
621 conjugated goat anti-human IgG (2015-05; SouthernBiotech) was diluted 1:8,000 in TBS-
622 T/3% BSA and added to plates for 30 min at room temperature. After washing with TBS-

623 T, plates were developed using 1-Step™ Ultra TMB-ELISA Substrate Solution (Thermo
624 Fisher Scientific) and absorbance was measured at 450 nm.
625
626 **mRNA synthesis**
627 Codon-optimized mRNAs encoding Wu1 S, Wu1 S-EABR, BA.5 S, and BA.5 S-EABR
628 constructs were synthesized by RNAcore (https://www.houstonmethodist.org/research-
629 cores/rnacore/) using proprietary manufacturing protocols as described[31]. In brief,
630 mRNAs were synthesized by T7 RNA polymerase-mediated in vitro transcription using
631 DNA templates encoding the immunogen open reading frame flanked by 5′ and 3'
632 untranslated regions and terminated by an encoded polyA tail. CleanCap 5' cap structures
633 (TriLink) were co-transcriptionally incorporated into the 5′ end. Uridine was completely
634 substituted with N1-methyl-pseudouridine to lower immunogenicity[62]. mRNAs were
635 purified by oligo-dT affinity purification and high-performance liquid chromatography
636 (HPLC) to remove double-stranded RNA contaminants[63]. Purified mRNAs were stored
637 at –80 °C.
638
639 **LNP encapsulation of mRNAs**
640 Purified mRNAs were formulated in LNP as described[31,64]. In brief, 1,2-distearoyl-*sn*-
641 glycero-3-phosphocholine, cholesterol, a PEG lipid, and an ionizable cationic lipid
642 dissolved in ethanol were rapidly mixed with an aqueous acidic solution containing the
643 mRNAs using an in-line mixer. The ionizable lipid and LNP composition are described in
644 the international patent application WO2017075531(2017). The post in-line solution was
645 dialyzed with PBS to remove ethanol and displace the acidic solution. Subsequently,

646 mRNA-LNP were measured for size (60-65 nm) and polydispersity (PDI < 0.075) by
647 dynamic light scattering (Malvern Nano ZS Zetasizer). The encapsulation efficiencies
648 were >97% as measured by the Quant-iT Ribogreen Assay (Invitrogen).
649
650 **Immunizations**
651 All animal procedures in this study were performed in compliance with the U.S.
652 Department of Agriculture's (USDA) Animal Welfare Act (9 CFR Parts 1, 2, and 3); the
653 Guide for the Care and Use of Laboratory Animals (Institute of Laboratory Animal
654 Resources, National Academy Press, Washington, D.C., 2011); and the National
655 Institutes of Health, Office of Laboratory Animal Welfare. Whenever possible, procedures
656 in this study were designed to avoid or minimize discomfort, distress, and pain to animals.
657 Animals were observed for signs of morbidity and/or mortality at least once daily,
658 according to animal welfare act and the Association for Assessment and Accreditation of
659 Laboratory Animal Care International (AAALACi). All mouse procedures were approved
660 by the Labcorp Institutional Animal Care and Use Committee (IACUC).
661
662 7-8 week-old female BALB/c mice (Charles River Laboratories) were purchased and
663 housed at Labcorp Drug Development, Denver, PA for immunization studies. All animals
664 were healthy upon receipt and were weighed and monitored during a 7-day acclimation
665 period before the start of the study. Mice were randomly assigned to experimental cohorts
666 of 10 animals. Up to 10 mice were co-housed together, and cages were kept in a climate-
667 controlled room at 63 to 77ºC at 50±20% relative humidity. Mice were provided Rodent
668 Diet #5001 (Purina Lab Diet) ad libitum.

669 2 μg of Wu1 S mRNA-LNP were administered to all cohorts of mice by IM injections on
670 days 0 and 28. On day 230, pre-vaccinated mice received different boosters by IM
671 injection: i) 2 μg Wu1 S mRNA-LNP; ii) 2 μg Wu1 S-EABR mRNA-LNP; iii) 1 μg Wu1 S
672 mRNA-LNP + 1 μg BA.5 S mRNA-LNP; iv) 1 μg Wu1 S-EABR mRNA-LNP + 1 μg BA.5
673 S-EABR mRNA-LNP. For bivalent boosters (iii and iv), the Wu1 and BA.5 S or S-EABR
674 mRNA-LNP were mixed prior to the IM injections. Serum samples for ELISAs and
675 neutralization assays were obtained on indicated days by retro-orbital bleeding. One
676 small drop of either 0.5% proparacaine hydrochloride ophthalmic solution or 0.5%
677 tetracaine hydrochloride ophthalmic solution was applied in the eye of the mouse prior to
678 performing retro-orbital blood collection. Eyes were alternated for each blood collection.
679 Euthanasia was performed in accordance with American Veterinary Medical Association
680 (AVMA) guidelines for euthanasia. Mice were individually placed in a CO2 chamber and
681 rendered unconscious. Mice were verified as unconscious by lack of response when toe
682 was pinched. Unconscious mice were subjected to bilateral jugular vein severance for
683 terminal exsanguination. Mice were placed back in the CO2 chamber until death
684 occurred. A double thoracotomy was performed as a second confirmation of death.
685

686 **Protein expression and purification**

687 Soluble SARS-CoV-2 S trimers (Wu1/D614G, BA.5, BQ.1.1, XBB.1)[32], RBDs (Wu1, BA.5,
688 BQ.1.1, XBB.1), and a prefusion-stabilized S2 protein[65] were expressed as described[37,66].
689 Briefly, Avi/His-tagged S trimers and His-tagged RBD and S2 proteins were purified from
690 transiently-transfected Expi293F cells (Gibco) by nickel affinity chromatography (HisTrap,
691 Cytiva) and size-exclusion chromatography (SEC) (Superose 6 Increase 10/300,

692 Cytiva)[33,37,66]. Peak fractions corresponding to S, RBD, or S2 proteins were pooled,
693 concentrated, and stored at 4ºC. Biotinylated S trimers for ELISAs were generated by co-
694 transfection of Avi/His-tagged S constructs with a plasmid encoding an endoplasmic
695 reticulum-directed BirA enzyme (kind gift from Michael Anaya, Caltech).
696
697 For heterotrimeric constructs, Wu1/BA.1 (HT2) and Wu1/BA.1/Delta (HT3) heterotrimers
698 were expressed via the addition of C-terminal tags and co-transfection of Expi293F cells
699 (Gibco) with specific plasmid DNA ratios. HT2 heterotrimers were produced by co-
700 transfecting a 1:1 plasmid DNA ratio of StrepII-tagged Wu1 S and His-tagged BA.1 S
701 constructs. HT3 heterotrimers were produced by co-transfecting a 1:1:1 plasmid DNA
702 ratio of StrepII-tagged Wu1 S, His-tagged BA.1 S, and D7324[47]-tagged Delta S
703 constructs. HT2 was sequentially purified using StrepTrap (Cytiva), HisTrap (Cytiva), and
704 SEC, while HT3 also underwent immunoaffinity chromatography using the D7324-specific
705 monoclonal Ab JR-52[47] (kind gift from James Robinson, Tulane University) before SEC.
706
707 The Wu1-His/Wu1-StrepII S homotrimer was generated by co-transfecting Expi293F cells
708 with a 1:1 plasmid DNA ratio of His-tagged Wu1 S and StrepII-tagged Wu1 S, followed by
709 purification as described for the HT2 heterotrimer. Single-tagged S homotrimers included
710 StrepII-tagged Wu1 S, His-tagged BA.1 S, and D7324-tagged Delta S, each purified using
711 their respective affinity chromatography steps followed by SEC.
712
713
714

715 **Single-particle cryo-EM sample preparation**

716 Grids of SARS-CoV-2 S homotrimers and heterotrimers were prepared at a protein
717 concentration of 2 mg/mL. Prior to freezing, fluorinated octylmaltoside solution (Anatrace)
718 was added to the S proteins at a final concentration of 0.02%(w/v). Three µL of S proteins
719 were immediately applied to Quantifoil 300 mesh 1.2/1.3 grids (Electron Microscopy
720 Sciences) that were freshly glow discharged with the PELCO easiGLOW (Ted Pella) for
721 60 seconds at 20 mA. Grids were blotted for 3 seconds using Whatman No.1 filter paper
722 with 0 blot force, 100% humidity and room temperature, and vitrified in 100% liquid ethane
723 using a Vitrobot Mark IV system (Thermo Fisher Scientific).

724

725 **Single-particle cryo-EM data collection and processing**

726 Single-particle cryo-EM datasets for SARS-CoV-2 S homotrimers and heterotrimers were
727 collected using SerialEM automatic data collection software[67] on a 300 keV Titan Krios
728 (Thermo Fisher Scientific) cryo-electron microscope equipped with a K3 direct electron
729 detector camera (Gatan). Movies were acquired in 40 frames with a defocus range of -1
730 to -3 µm and a total dosage of 60 electrons per $Å^2$ using the 3 by 3 beam image shift
731 pattern with 3 exposures per hole in the super-resolution mode at a pixel size of 0.416 Å.
732 Data processing workflows are outlined in Figure S10. For all datasets, motion correction
733 was done with patch motion correction with a binning factor of 2 and contrast transfer
734 function (CTF) parameters were estimated with Patch CTF in cryoSPARC[68]. Particles with
735 a diameter of 100 to 200 Å were picked with blob picker, inspected, extracted, and finally
736 classified with 2D classification in cryoSPARC[68]. Ice particles, junk particles, and particles
737 with preferred orientations were discarded, and the remaining particles were used for *ab*

738 *initio* reconstruction of three to four volumes. These reconstructions were further refined
739 with heterogeneous refinement in cryoSPARC[68]. Depending on the state for the receptor-
740 binding domains (RBDs) in the reconstructions, particles were combined for
741 homogeneous and non-uniform refinements to obtain the final reconstructions in
742 cryoSPARC[68].
743
744 **ELISAs**
745 ELISAs were performed as described[31,44]. To analyze serum binding to S trimers, pre-
746 blocked streptavidin-coated Nunc® MaxiSorp™ 384-well plates (ThemoFisher Scientific)
747 were coated with 5 µg/mL biotinylated S trimers in TBS-T/3% BSA for 1 hour at room
748 temperature. To analyze serum binding to RBDs or S2, Nunc® MaxiSorp™ 384-well
749 plates (Sigma) were coated with 2.5 µg/mL RBD or S2 in 0.1 M $NaHCO_3$ pH 9.8 and
750 incubated overnight at 4°C. Plates were blocked with TBS-T/3% BSA for 1 hour at room
751 temperature followed by removal of the blocking buffer by aspiration. Serum samples from
752 immunized mice were diluted 1:100, 4-fold serially diluted in TBS-T/3% BSA, and added
753 to plates. After a 3-hour incubation at room temperature, plates were washed with TBS-
754 T using an automated plate washer. HRP-conjugated goat anti-mouse IgG (715-035-150;
755 Jackson ImmunoResearch) was diluted 1:100,000 in TBS-T/3% BSA and added to plates
756 for 1 hour at room temperature. After washing with TBS-T, plates were developed using
757 SuperSignal™ ELISA Femto Maximal Signal Substrate (Thermo Fisher Scientific) and
758 absorbance was measured at 425 nm. Area under the curve (AUC) calculations for
759 binding curves were performed using GraphPad Prism 9.3.1 assuming a one-site binding
760 model with a Hill coefficient as described[69].

761 **Neutralization assays**

762 Lentivirus-based SARS-CoV-2 pseudoviruses were generated as described[35,36] using S
763 proteins from the Wu1/D614G, BA.1, BA.5, BQ.1.1, and XBB.1 variants in which the C-
764 terminal 21 residues of the S cytoplasmic tails were removed[35]. Serum samples from
765 immunized mice were heat-inactivated for 30 min at 56ºC. Three-fold serial dilutions of
766 heat-inactivated samples were incubated with pseudoviruses for 1 hour at 37ºC, followed
767 by addition of the serum-virus mixtures to pre-seeded HEK293T-ACE2 target cells. After
768 48-hour incubation at 37ºC, BriteLite Plus substrate (Perkin Elmer) was added and
769 luminescence was measured. Half-maximal inhibitory dilutions (ID_{50}s) were calculated
770 using 4-parameter non-linear regression analysis in AntibodyDatabase[70] and ID_{50} values
771 were rounded to three significant figures.

772

773 **Ab depletions**

774 HiTrap™ NHS-activated resin (Cytiva) was coupled to purified SARS-CoV-2 Wu1 RBD or
775 a mock protein (HIV-1 gp120) at a 10 mg/mL concentration and stored in PBS
776 supplemented with 0.02% sodium azide at 4°C. For Ab depletions, 50 µL dry worth of
777 RBD-coupled resin were aliquoted into microcentrifuge tubes and spun down at 13,000 x
778 g for 2 minutes. The supernatant was discarded. The resin was washed with 100 µL of
779 sterile PBS to remove excess PBS-azide solution. The supernatant was again discarded.
780 10 µL of mouse serum was then diluted in 90 µL PBS, and added to the resin. The tubes
781 were mixed and incubated at room temperature for 10 minutes. The resin-serum mixture
782 was spun down at 13,000 x g for 7 minutes to allow the resin to settle, and 90 µL of the
783 supernatant was transferred into a fresh microcentrifuge tube. To ensure no resin was

784 present in the final sample, the collection tube was spun down again, and supernatant
785 was transferred to a fresh microcentrifuge tube. Sterile PBS was added for a final volume
786 of 200 µL. Prior to neutralization assays, the Ab depleted serum samples were heat-
787 inactivated at 56°C for 30 minutes.
788
789 **Deep mutational scanning**
790 DMS studies to map RBD epitopes recognized by serum Abs were performed in biological
791 duplicates using independent mutant RBD yeast libraries (Wu1[42,71] and XBB.1.5 RBD[43]
792 libraries were generously provided by Tyler Starr, University of Utah) as
793 described[44,66,72,73]. Briefly, yeast libraries were stained with serum Abs, labeled with a
794 secondary Ab (115-605-008, Jackson ImmunoResearch), and then processed using a
795 Sony SH800 cell sorter. Cells were gated to capture RBD mutants that had reduced Ab
796 binding for a relatively high degree of RBD expression. Ab-escaped cells were expanded
797 for DNA extraction and Illumina sequencing was done as described[44,72,73]. Raw
798 sequencing data are available on the NCBI SRA under BioProject PRJNA1067836.
799 Escape fractions were computed using previously described processing steps[44,72,73] and
800 implemented using a Swift DMS program available from authors upon request.
801
802 Escape map visualizations shown as static line plots, logo plots and structural depictions
803 were all created using Swift DMS as previously described[41,44,73]. In some visualizations,
804 RBD sites were categorized based on epitope region, which were defined as class 1 (pink)
805 (RBD residues 403, 405, 406, 417, 420, 421, 453, 455-460, 473-478, 486, 487, 489, 503,
806 504), class 2 (purple) (residues 472, 479, 483-485, 490-495), class 3 (blue) (residues

807 341, 345, 346, 437-450, 496, 498-501), class 4 (orange) (residues 365-390, 408)[74], or
808 class 5 (green) (352-357, 396, 462-468)[41]. Structural visualizations were performed using
809 an RBD surface (PDB 6M0J) colored by the site-wise escape metric at each site as
810 described[44].
811
812 **Statistical analysis**
813 Statistically significant titer differences between immunized cohorts of BALB/c mice (10
814 mice per cohort) for ELISAs were determined using analysis of variance (ANOVA) test
815 followed by Tukey's multiple comparison post hoc test calculated using Graphpad Prism
816 9.3.1. Titer differences between immunized cohorts of BALB/c mice for Wu1, BA.5,
817 BQ.1.1, and XBB.1 neutralization assays were determined using the non-parametric
818 Kruskal-Wallis test followed by Dunn's multiple comparison post hoc test calculated using
819 Graphpad Prism 9.3.1. For BA.1 neutralization titers, statistically significant differences
820 were determined using the non-parametric two-tailed Mann-Whitney test calculated using
821 Graphpad Prism 9.3.1.
822

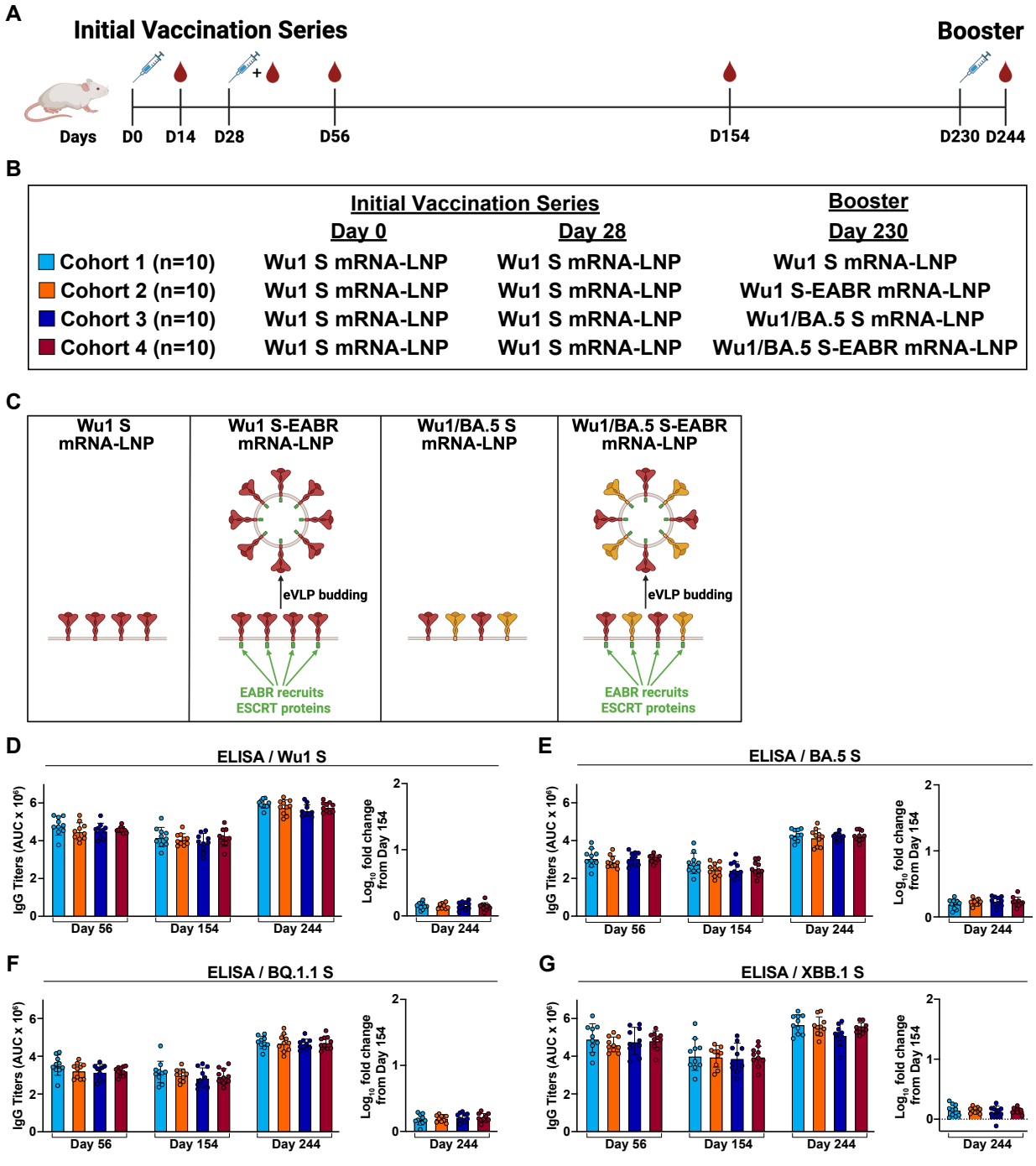

Figure 1. Monovalent and bivalent boosters elicit similar Ab binding responses against variant S trimers in pre-vaccinated mice. A) Immunization schedule in BALB/c mice. Blood samples were collected on days 14, 56, 154, and 244. This panel was created using BioRender.com. **B)** Immunization regimens for each cohort. All cohorts were initially

828 vaccinated with 2 µg of Wu1 S mRNA-LNP on days 0 and 28 by IM injection. Pre-
829 vaccinated mice received different boost immunogens on day 230 by IM injection. Cohorts
830 1-4 received 2 µg of monovalent Wu1 S mRNA-LNP (cyan), monovalent Wu1 S-EABR
831 mRNA-LNP (orange), bivalent Wu1/BA.5 S mRNA-LNP (blue), or bivalent Wu1/BA.5 S-
832 EABR mRNA-LNP (maroon), respectively. **C)** Schematic showing the different boost
833 immunogens that were administered on day 230. Wu1 S mRNA-LNP immunization results
834 in cell surface presentation of membrane-anchored Wu1 S trimers. Wu1 S-EABR mRNA-
835 LNP immunization results in dual presentation of Wu1 S trimers on cell surfaces and on
836 eVLPs that are secreted after budding from the plasma membrane. eVLP formation is
837 induced by EABR-mediated recruitment of host cell proteins from the ESCRT pathway.
838 Bivalent Wu1/BA.5 S mRNA-LNP immunization results in cell surface presentation of
839 membrane-anchored Wu1 and BA.5 S trimers. Wu1/BA.5 S-EABR mRNA-LNP
840 immunization results in dual presentation of Wu1 and BA.5 S trimers on cell surfaces and
841 eVLPs that bud from the plasma membrane. S trimers are shown as homotrimers for both
842 monovalent and bivalent boost immunogens. This panel was created
843 using BioRender.com. **D-G)** ELISA data from indicated time points for antisera from
844 individual mice (colored circles) presented as the geometric mean (bars) and standard
845 deviation (horizontal lines) of area under the curve (AUC) values. ELISAs evaluated
846 binding of purified Ss from the **D)** Wu1, **E)** BA.5, **F)** BQ.1.1, and **G)** XBB.1 variants. The
847 $\log_{10}$-fold change in binding titers from day 154 to day 244 is also shown for each S
848 (plotted as mean (bars) and standard deviation (horizontal lines)).
849

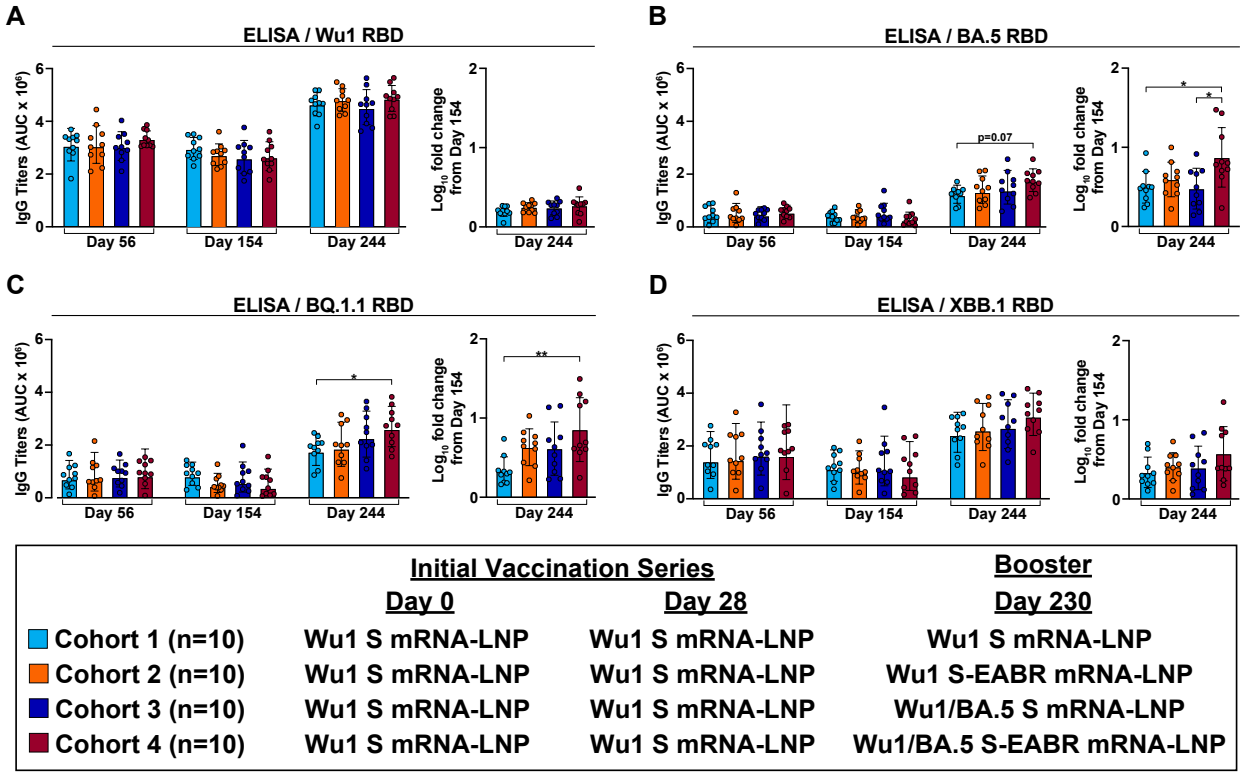

	Initial Vaccination Series		Booster
	Day 0	Day 28	Day 230
Cohort 1 (n=10)	Wu1 S mRNA-LNP	Wu1 S mRNA-LNP	Wu1 S mRNA-LNP
Cohort 2 (n=10)	Wu1 S mRNA-LNP	Wu1 S mRNA-LNP	Wu1 S-EABR mRNA-LNP
Cohort 3 (n=10)	Wu1 S mRNA-LNP	Wu1 S mRNA-LNP	Wu1/BA.5 S mRNA-LNP
Cohort 4 (n=10)	Wu1 S mRNA-LNP	Wu1 S mRNA-LNP	Wu1/BA.5 S-EABR mRNA-LNP

Figure 2. Bivalent S-EABR mRNA-LNP booster elicits potent Ab responses targeting Omicron RBDs. A-D) RBD binding titers for antisera from pre-vaccinated mice that received booster immunizations with 2 µg of monovalent Wu1 S mRNA-LNP (cyan), 2 µg of monovalent Wu1 S-EABR mRNA-LNP (orange), 2 µg of bivalent Wu1/BA.5 S mRNA-LNP (blue), or 2 µg of bivalent Wu1/BA.5 S-EABR mRNA-LNP (maroon) (immunization schedule in Fig. 1A-B). ELISA data are shown for indicated time points for antisera from individual mice (colored circles) presented as the geometric mean (bars) and standard deviation (horizontal lines) of area under the curve (AUC) values. ELISAs evaluated binding of RBDs from the **A)** Wu1, **B)** BA.5, **C)** BQ.1.1, and **D)** XBB.1 SARS-CoV-2 variants. The $\log_{10}$-fold change in binding titers from day 154 to day 244 is also shown for each RBD (plotted as mean (bars) and standard deviation (horizontal lines)).

862 Significant differences between cohorts linked by horizontal lines are indicated by

863 asterisks: $p<0.05$ = *, $p<0.01$ = **.

864

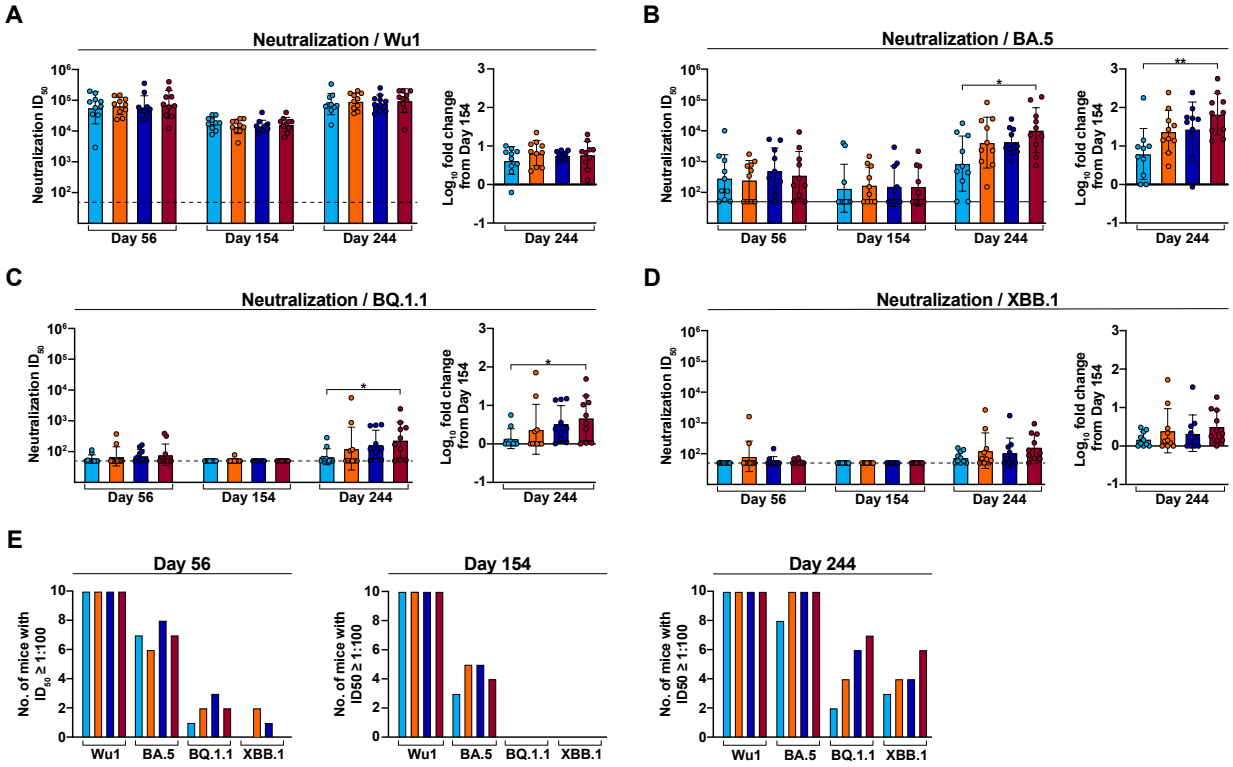

	Initial Vaccination Series		Booster
	Day 0	Day 28	Day 230
Cohort 1 (n=10)	Wu1 S mRNA-LNP	Wu1 S mRNA-LNP	Wu1 S mRNA-LNP
Cohort 2 (n=10)	Wu1 S mRNA-LNP	Wu1 S mRNA-LNP	Wu1 S-EABR mRNA-LNP
Cohort 3 (n=10)	Wu1 S mRNA-LNP	Wu1 S mRNA-LNP	Wu1/BA.5 S mRNA-LNP
Cohort 4 (n=10)	Wu1 S mRNA-LNP	Wu1 S mRNA-LNP	Wu1/BA.5 S-EABR mRNA-LNP

Figure 3. Bivalent Wu1/BA.5 S-EABR mRNA-LNP booster elicits higher neutralizing responses against Omicron subvariants. A-D) Neutralization titers for antisera from pre-vaccinated mice that received booster immunizations with 2 µg of monovalent Wu1 S mRNA-LNP (cyan), 2 µg of monovalent Wu1 S-EABR mRNA-LNP (orange), 2 µg of bivalent Wu1/BA.5 S mRNA-LNP (blue), or 2 µg of bivalent Wu1/BA.5 S-EABR mRNA-LNP (maroon) (immunization schedule in Fig. 1A-B). Neutralization data are shown for indicated time points for antisera from individual mice (colored circles) presented as the geometric mean (bars) and standard deviation (horizontal lines) of ID_{50} values. Results are shown for **A)** Wu1, **B)** BA.5, **C)** BQ.1.1, and **D)** XBB.1 pseudoviruses. Dashed

875 horizontal lines correspond to the background values representing the limit of detection
876 for neutralization assays (ID_{50} = 1:50). The log_{10}-fold change in neutralization titers from
877 day 154 to day 244 is also shown for each pseudovirus (plotted as mean (bars) and
878 standard deviation (horizontal lines)). Significant differences between cohorts linked by
879 horizontal lines are indicated by asterisks: $p<0.05$ = *, $p<0.01$ = **. **E)** Number of mice in
880 each cohort that reached an $ID_{50} \leq$ 1:100 against each variant on days 56 (left), 154
881 (middle), and 244 (right).
882

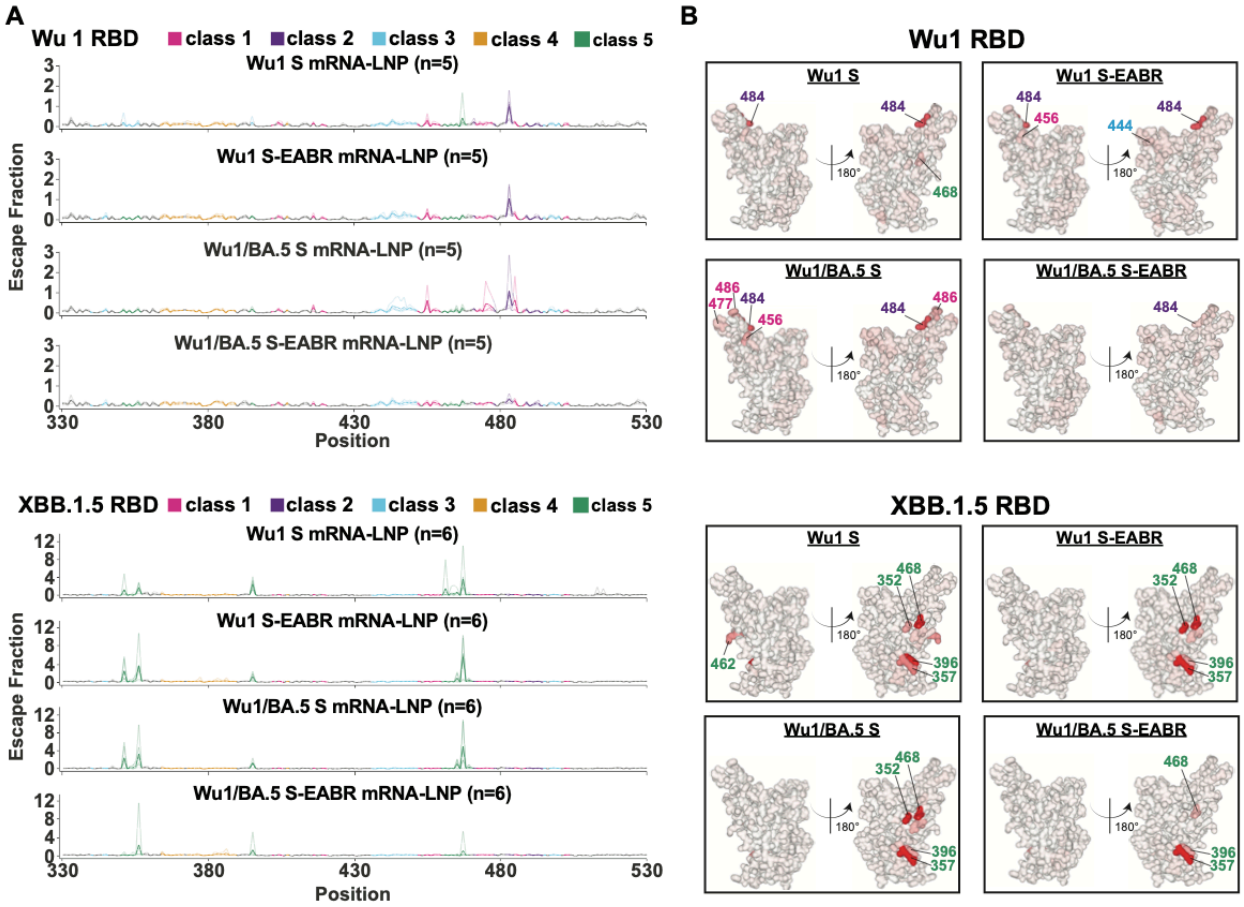

Figure 4. Bivalent S-EABR mRNA-LNP booster induces polyclass Ab responses. Sera for DMS studies were derived from pre-vaccinated mice that received booster immunizations with 2 µg of monovalent Wu1 S mRNA-LNP, monovalent Wu1 S-EABR mRNA-LNP, bivalent Wu1/BA.5 S mRNA-LNP, or bivalent Wu1/BA.5 S-EABR mRNA-LNP (immunization schedule in Fig. 1A-B). DMS was performed for 6 serum samples for each cohort, which were selected based on XBB.1 neutralization activity (1st, 2nd, 3rd, 5th, 6th, and 10th best neutralizer from each cohort). For the Wu1 RBD library, only five DMS profiles were obtained for each cohort. **A)** Line plots for DMS results using Wu1 (top) or XBB.1.5 (bottom) RBD libraries for sera from pre-vaccinated mice that received the indicated boost immunogens. The x axes display the RBD residue numbers, and the y

894 axes show the sum of the Ab escape of all mutations at a site (larger numbers indicating
895 increased Ab escape). Each faint line shows one antiserum with heavy lines representing
896 the average across the n = 5 (top) or n = 6 (bottom) sera in each cohort. Lines are colored
897 differently for RBD epitopes within different RBD epitope classes[33,40] (color definitions
898 shown in legend above line plots; epitopes are shown in Fig. S2; gray color for residues
899 not assigned to an epitope). **B)** The average site-total Ab escape for the Wu1 (top) or
900 XBB.1.5 (bottom) RBD libraries for pre-vaccinated mice that received the indicated boost
901 immunogens mapped to the Wu1 RBD surface (PDB: 6M0J). Gray coloring indicates no
902 escape, and red coloring indicates escape. Lines with numbers colored according to
903 epitope class indicate RBD positions with the most escape.

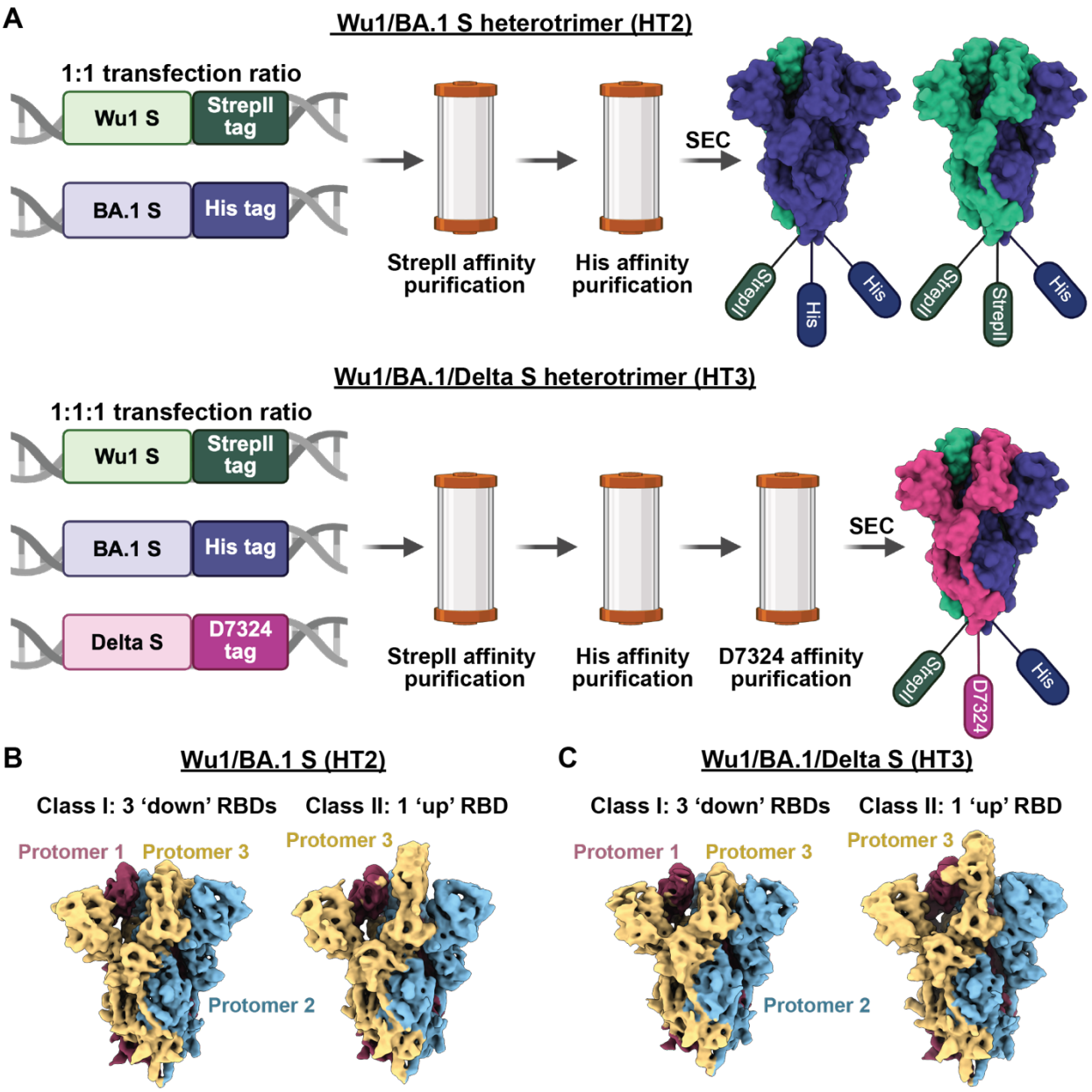

D

Trimers/ Heterotrimers \ Conformational states	0 'up' RBD 3 'down' RBDs	1 'up' RBD 2 'down' RBDs
Wu1/BA.1 S (HT2)	✔	✔
Wu1/BA.1/Delta S (HT3)	✔	✔
Wu1 S Tag Control (StrepII/His)	✔	✔
Wu1 S	✔	✔
BA.1 S	✔	✔
Delta S	✔	✔

904

905 **Figure 5. Heterotrimer S formation occurs for soluble constructs. A)** Schematic for
906 the generation and purification of soluble SARS-CoV-2 Wu1/BA.1 (HT2) and
907 Wu1/BA.1/Delta (HT3) S heterotrimers. HT2 heterotrimers were generated by co-
908 transfection of StrepII-tagged Wu1 S and His-tagged BA.1 S constructs at a 1:1 DNA
909 ratio, while HT3 heterotrimers were produced by co-transfecting StrepII-tagged Wu1 S,
910 His-tagged BA.1 S, and D7324-tagged Delta S constructs at a 1:1:1 ratio. Each
911 heterotrimer was sequentially purified using affinity chromatography specific for each tag
912 (StrepII, His, or JR-52) to ensure incorporation of distinct protomers. This panel was
913 created using BioRender.com. **B)** Cryo-EM density maps for Wu1/BA.1 HT2 S class I with
914 3 'down' RBDs (3.8 Å resolution) and class II with 1 'up' RBD (3.8 Å resolution). **C)** 4.0 Å
915 and 3.9 Å resolution cryo-EM density maps for Wu1/BA.1/Delta HT3 S with 3 'down' RBDs
916 and 1 'up' RBD. **D)** Table summarizing S heterotrimer and control homotrimer
917 conformational states.
918

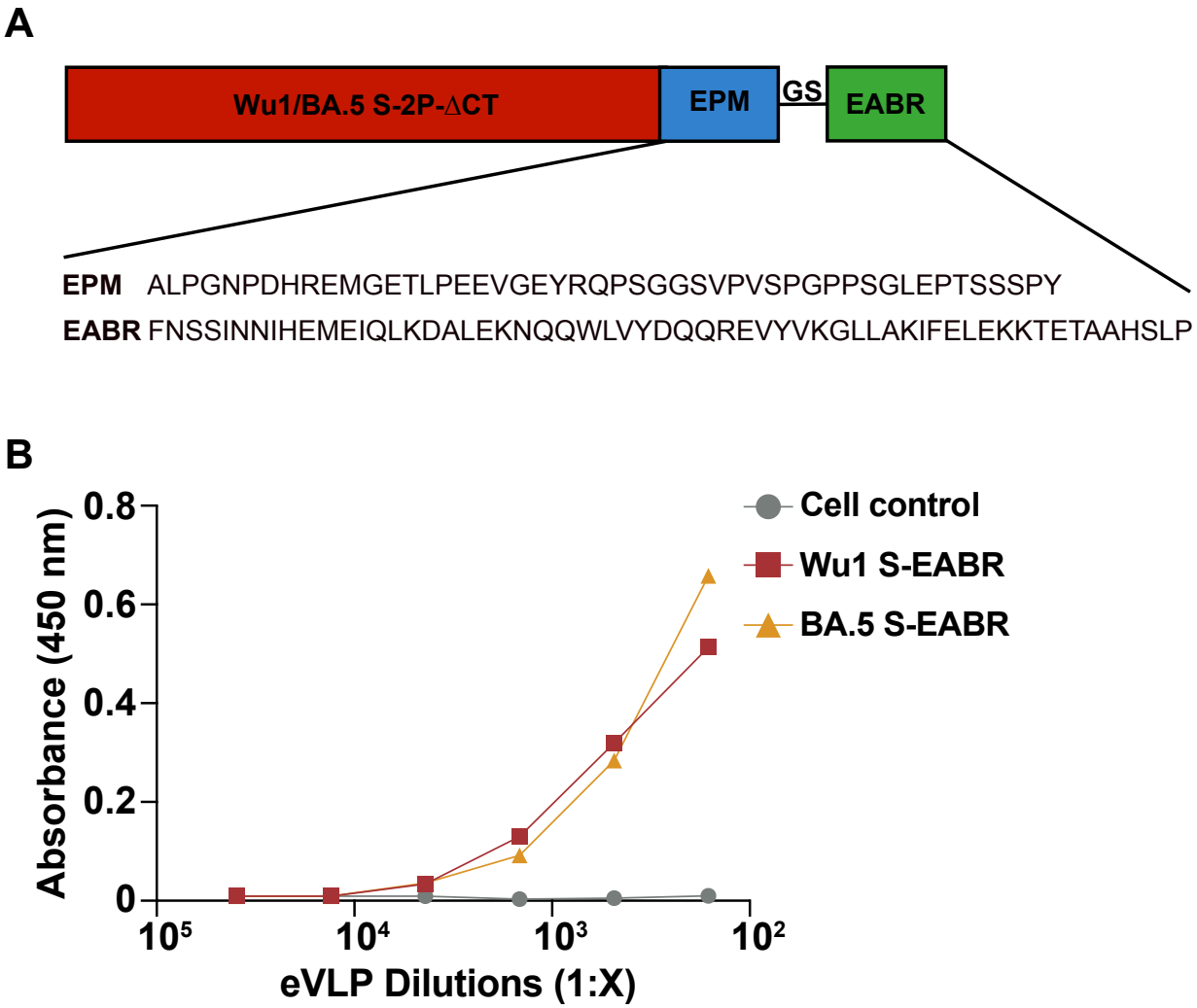

Figure S1. Wu1 and BA.5 S-EABR constructs induce efficient eVLP budding. A) Design and sequence information for SARS-CoV-2 S-EABR constructs. Top: The Wu1 and BA.5 S (including a furin cleavage site, 2P stabilizing substitutions, the D614G substitution, and ΔCT, a cytoplasmic tail deletion) were fused to an EPM sequence, a $(Gly)_3Ser$ (GS) spacer, and an EABR sequence. EPM = Endocytosis prevention motif. GS = $(Gly)_3Ser$ linker. EABR = ESCRT- and ALIX-binding region. Bottom: EPM and EABR sequence information. **B)** DNA plasmids encoding Wu1 S-EABR (red) or BA.5 S-EABR (orange) constructs were transfected into HEK293T cells. 48 hours post-transfection, transfected cell culture supernatants were harvested, and eVLPs were purified by

929 ultracentrifugation on a 20% sucrose cushion. Purified eVLP samples were serially
930 diluted, directly coated onto 96-well plates, and eVLP-associated S protein levels were
931 quantified by ELISA.
932

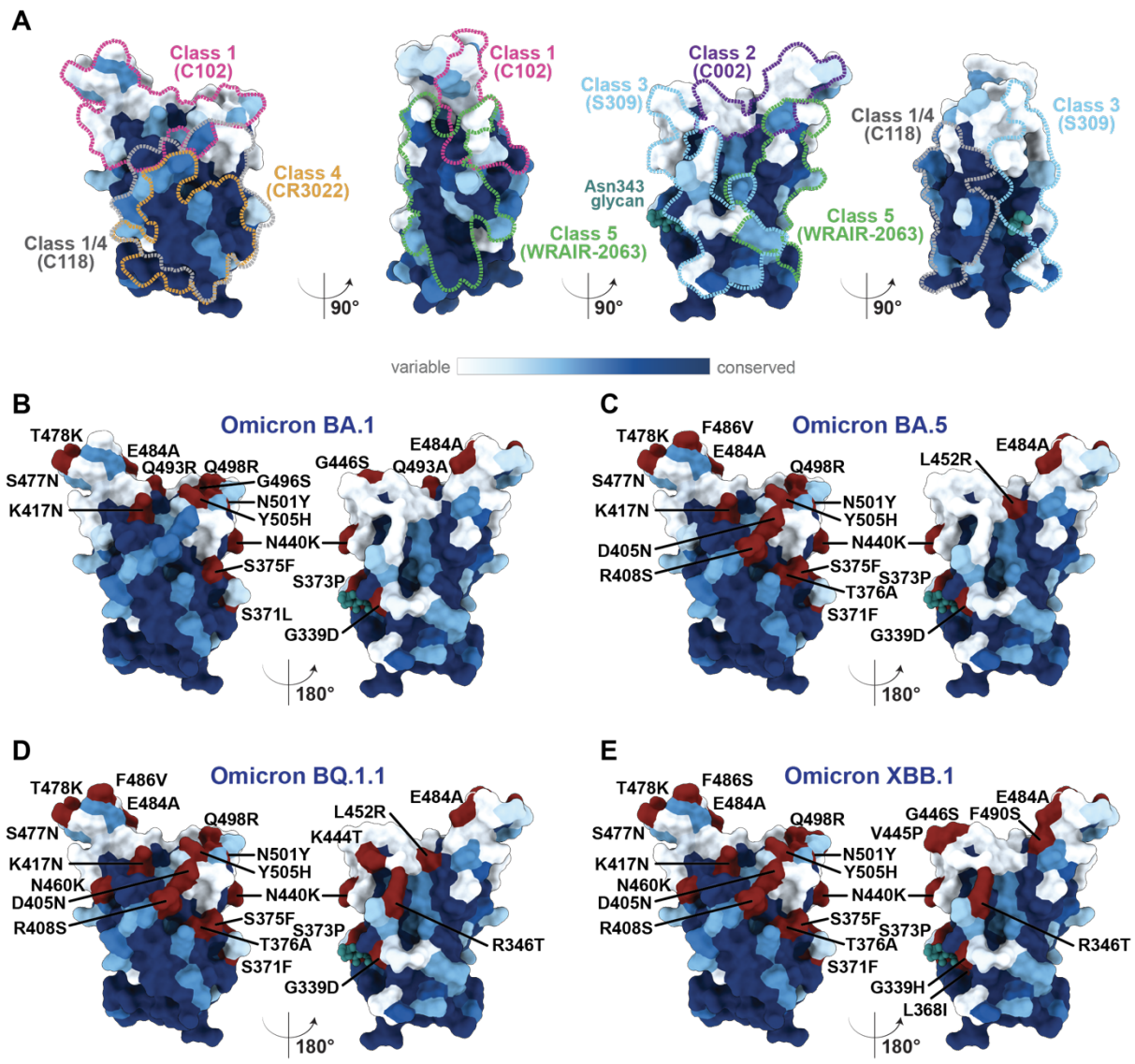

933

934 **Figure S2. Sarbecovirus RBD sequence conservation. A)** Sequence conservation of
935 16 sarbecovirus RBDs calculated with ConSurf[75] and plotted on a surface representation
936 of a SARS-CoV-2 RBD (PDB 7BZ5). Anti-RBD class 1, 2, 3, 4, 1/4, and 5 Ab epitopes are
937 outlined with dotted lines in different colors using structural information from
938 representative structures of mAb bound to SARS-CoV-2 S or RBD (C102: PDB 7K8M;
939 C002: PDB 7K8T, S309: PDB 7JX3; CR3022: PDB 7LOP; C118: PDB 7RKV; WRAIR-

940 2063: PDB 8EOO). SARS-CoV-2 RBD substitutions (colored in red) in Omicron **B)** BA.1,

941 **C)** BA.5, **D)** BQ.1.1, and **E)** XBB.1 variants plotted on the RBD sequence conservation

942 plot.

943

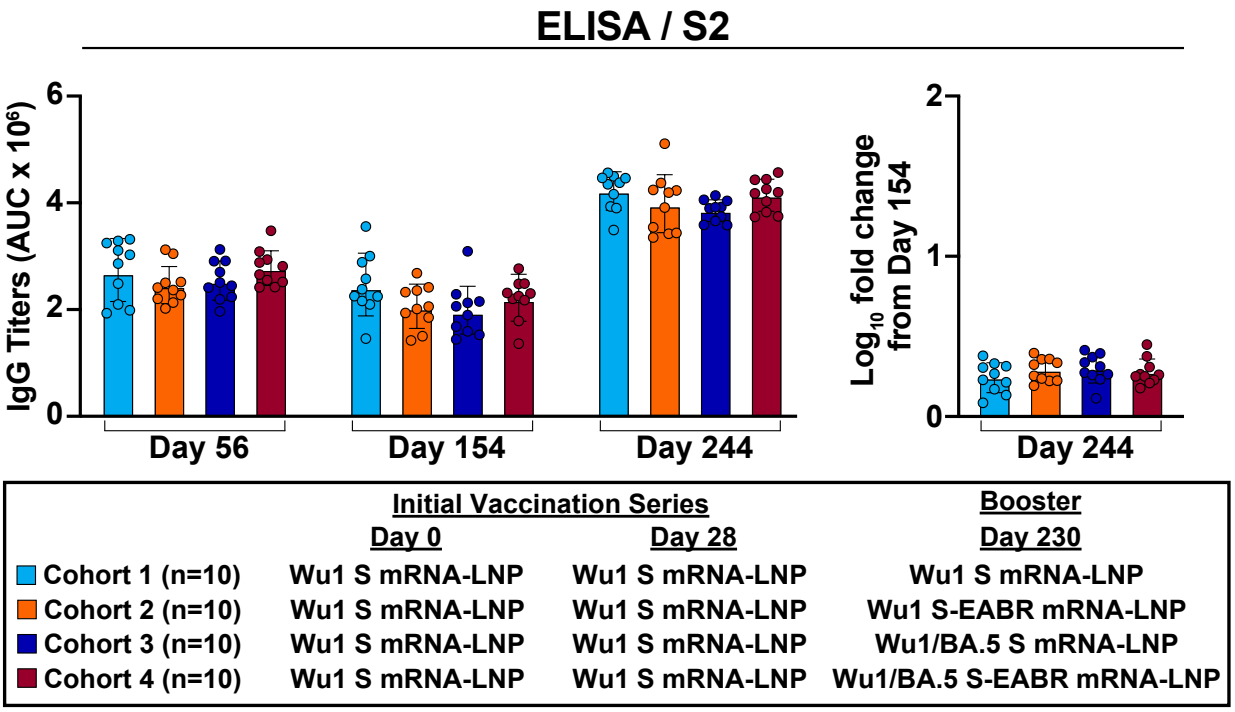

Figure S3. Primary vaccinations and booster immunizations elicit potent anti-S2 binding responses. S2 binding titers for antisera from pre-vaccinated mice that received booster immunizations with 2 µg of monovalent Wu1 S mRNA-LNP (cyan), 2 µg of monovalent Wu1 S-EABR mRNA-LNP (orange), 2 µg of bivalent Wu1/BA.5 S mRNA-LNP (blue), or 2 µg of bivalent Wu1/BA.5 S-EABR mRNA-LNP (maroon). ELISA data for binding of Wu1 S2 are shown for indicated time points for antisera from individual mice (colored circles) presented as the geometric mean (bars) and standard deviation (horizontal lines) of area under the curve (AUC) values. The $\log_{10}$-fold change in binding titers from day 154 to day 244 is also shown (plotted as mean (bars) and standard deviation (horizontal lines)).

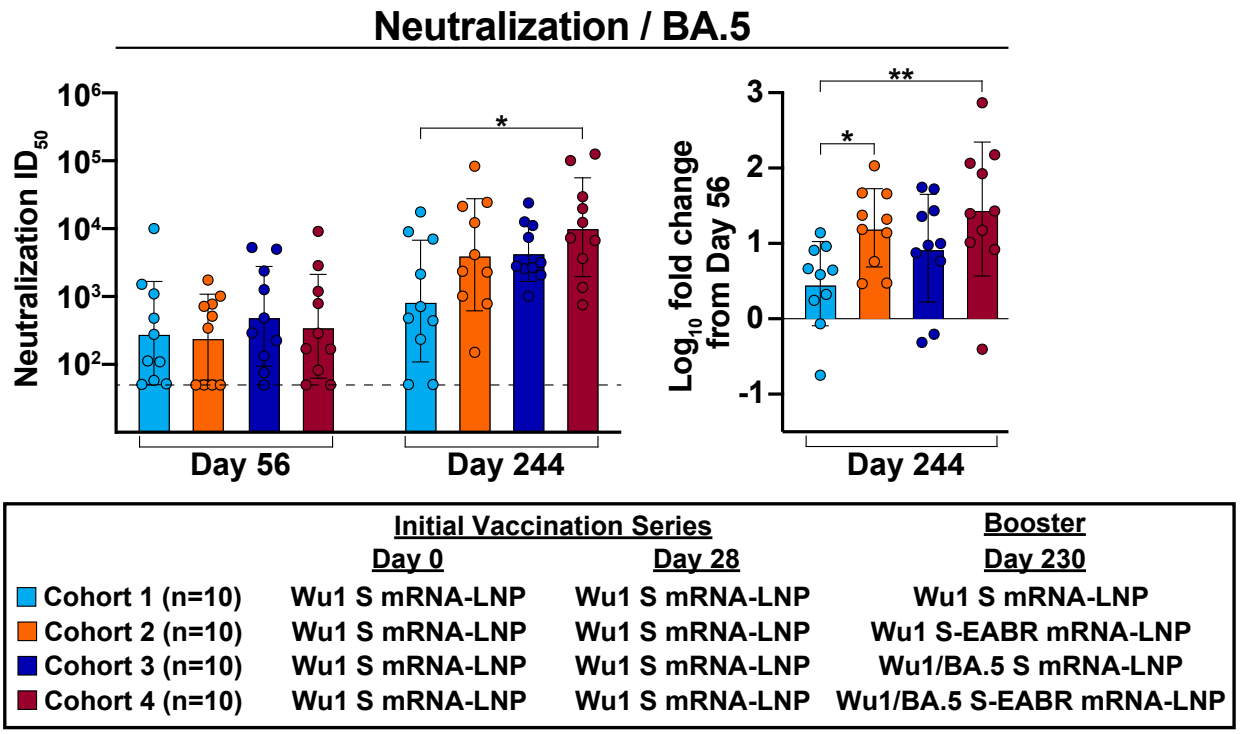

Figure S4. Monovalent and bivalent S-EABR mRNA-LNP boosters elicit higher increases in BA.5 neutralization compared to conventional S mRNA-LNP boosters. Neutralization titers for antisera from pre-vaccinated mice that received booster immunizations with 2 µg of monovalent Wu1 S mRNA-LNP (cyan), 2 µg of monovalent Wu1 S-EABR mRNA-LNP (orange), 2 µg of bivalent Wu1/BA.5 S mRNA-LNP (blue), or 2 µg of bivalent Wu1/BA.5 S-EABR mRNA-LNP (maroon) (immunization schedule in Fig. 1A-B). BA.5 neutralization data are shown for indicated time points for antisera from individual mice (colored circles) presented as the geometric mean (bars) and standard deviation (horizontal lines) of ID_{50} values. Dashed horizontal lines correspond to the background values representing the limit of detection for neutralization assays (ID_{50} = 1:50). The log_{10}-fold change in neutralization titers from day 56 to day 244 is also shown (plotted as mean (bars) and standard deviation (horizontal lines)). Significant differences

969 between cohorts linked by horizontal lines are indicated by asterisks: $p<0.05$ = *, $p<0.01$

970 = **.

971

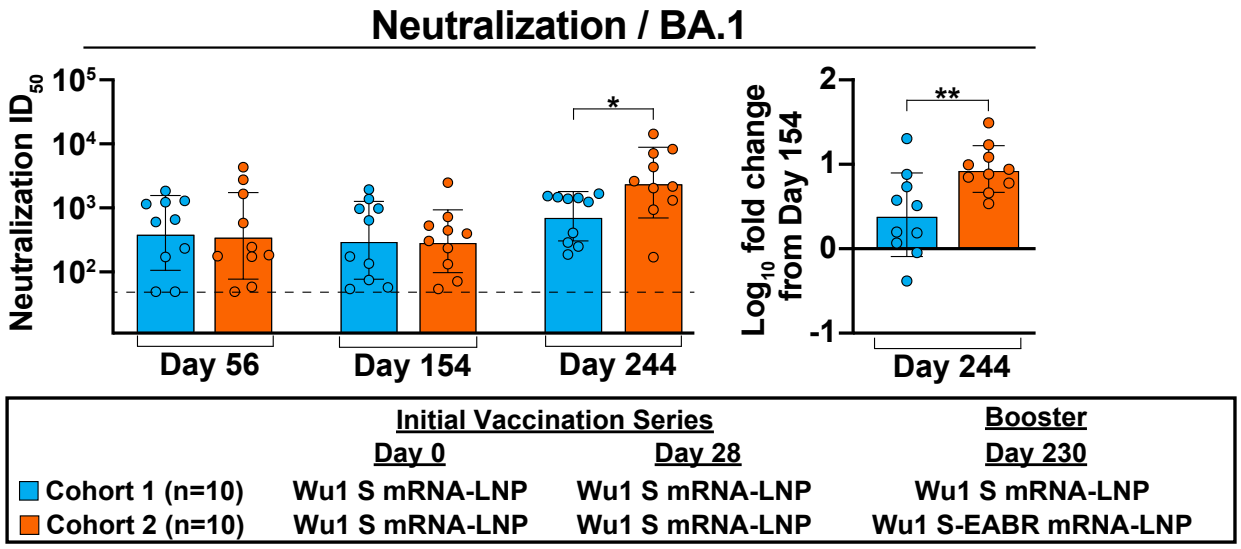

Figure S5. Monovalent Wu1 S-EABR mRNA-LNP booster elicits improved neutralizing responses against BA.1 variant. Neutralization titers for antisera from pre-vaccinated mice that received booster immunizations with 2 µg of monovalent Wu1 S mRNA-LNP (cyan) or monovalent Wu1 S-EABR mRNA-LNP (orange). Neutralization data are shown for indicated time points for antisera from individual mice (colored circles) presented as the geometric mean (bars) and standard deviation (horizontal lines) of ID_{50} values against BA.1 pseudovirus. Dashed horizontal lines correspond to the limit of detection for neutralization assays (ID_{50} = 1:50). The log_{10}-fold change in neutralization titers from day 154 to day 244 is also shown (plotted as mean (bars) and standard deviation (horizontal lines)). Significant differences between cohorts linked by horizontal lines are indicated by asterisks: $p<0.05$ = *.

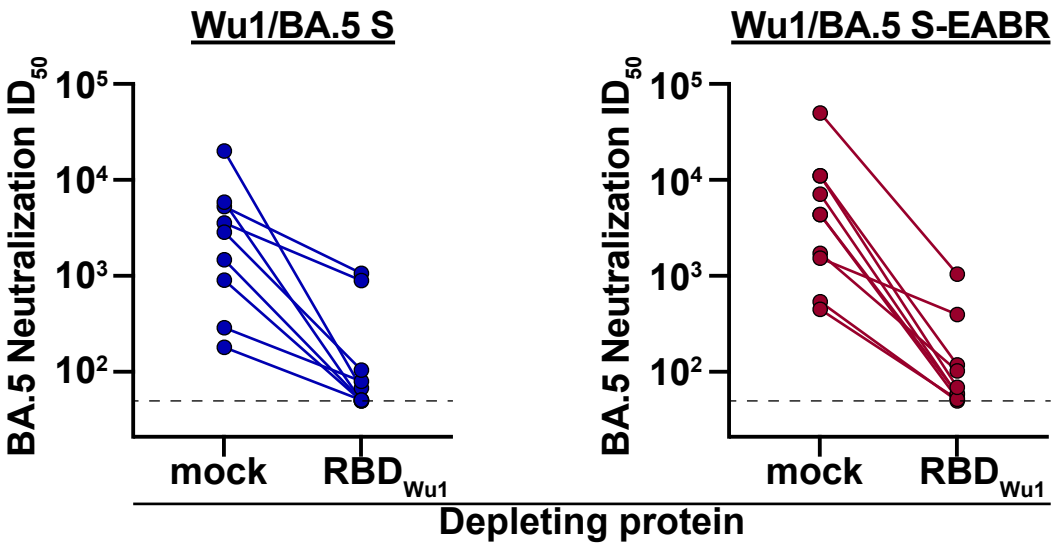

984

985 **Figure S6. Depleting bivalent booster-induced antisera with Wu1 RBD reduces**
986 **BA.5 neutralizing activity.** Day 244 serum samples obtained from pre-vaccinated mice
987 that received booster immunizations with 2 µg of bivalent Wu1/BA.5 S mRNA-LNP (blue)
988 or 2 µg of bivalent Wu1/BA.5 S-EABR mRNA-LNP (maroon) were depleted using a mock
989 protein (HIV-1 gp120; left) or Wu1 RBD (right). The neutralizing activity of the depleted
990 antisera was measured against BA.5 pseudovirus. Neutralization data are shown as ID_{50}
991 values for individual mice (colored circles). Data points for individual mice following mock
992 or Wu1 RBD depletions are connected by colored lines. Dashed horizontal lines
993 correspond to the limit of detection for neutralization assays (ID_{50} = 1:50).

994

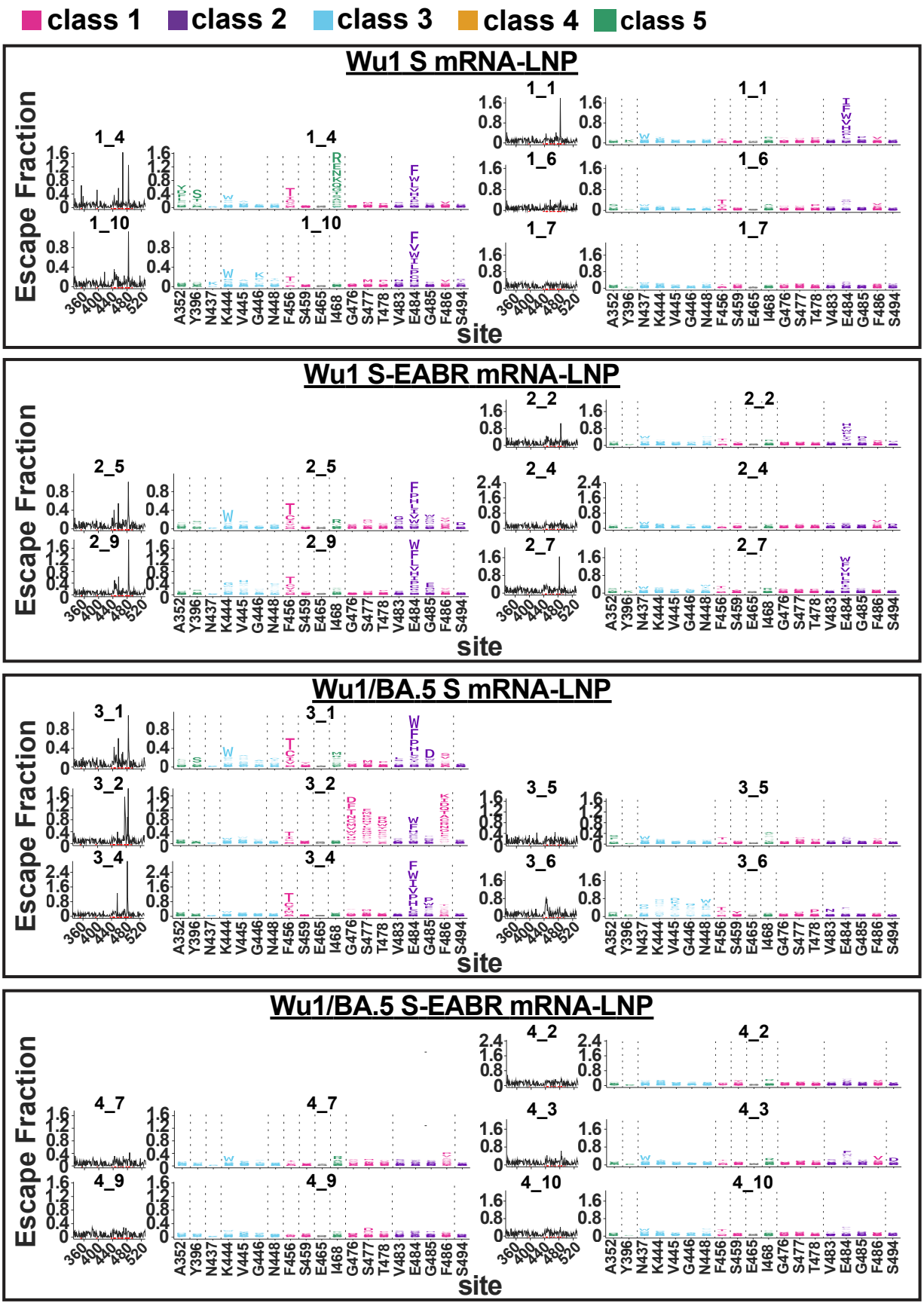
class 1
class 2
class 3
class 4
class 5
Wu1 S mRNA-LNP
Wu1 S-EABR mRNA-LNP
Wu1/BA.5 S mRNA-LNP
Wu1/BA.5 S-EABR mRNA-LNP
Escape Fraction
site
A352 Y396 N437 K444 V445 G446 N448 F456 S459 E465 I468 G476 S477 T478 V483 E484 G485 F486 S494

995

996 **Figure S7. Bivalent S-EABR mRNA-LNP booster induces polyclass Ab responses**
997 **against Wu1 RBD.** Sera for DMS studies were derived from pre-vaccinated mice that
998 received booster immunizations with 2 µg of monovalent Wu1 S mRNA-LNP, monovalent
999 Wu1 S-EABR mRNA-LNP, bivalent Wu1/BA.5 S mRNA-LNP, or bivalent Wu1/BA.5 S-
1000 EABR mRNA-LNP (immunization schedule in Fig. 1A-B). Line (left) and logo plots (right)
1001 are shown for DMS results for individual sera from pre-vaccinated mice that received the
1002 indicated boost immunogens. DMS was performed using a Wu1 RBD library. The x axes
1003 of the line and logo plots display the RBD residue numbers. The y axis of the line plots
1004 shows the sum of the Ab escape of all mutations at a site (larger numbers indicating
1005 increased Ab escape). Sites with the strongest Ab escape are shown in logo plots, with
1006 tall letters representing the most frequent mutations at a site. Logo plots are colored
1007 differently for RBD epitopes within different classes[33,40,41] (epitopes are shown in Fig. S2;
1008 gray color for residues not assigned to an epitope).
1009

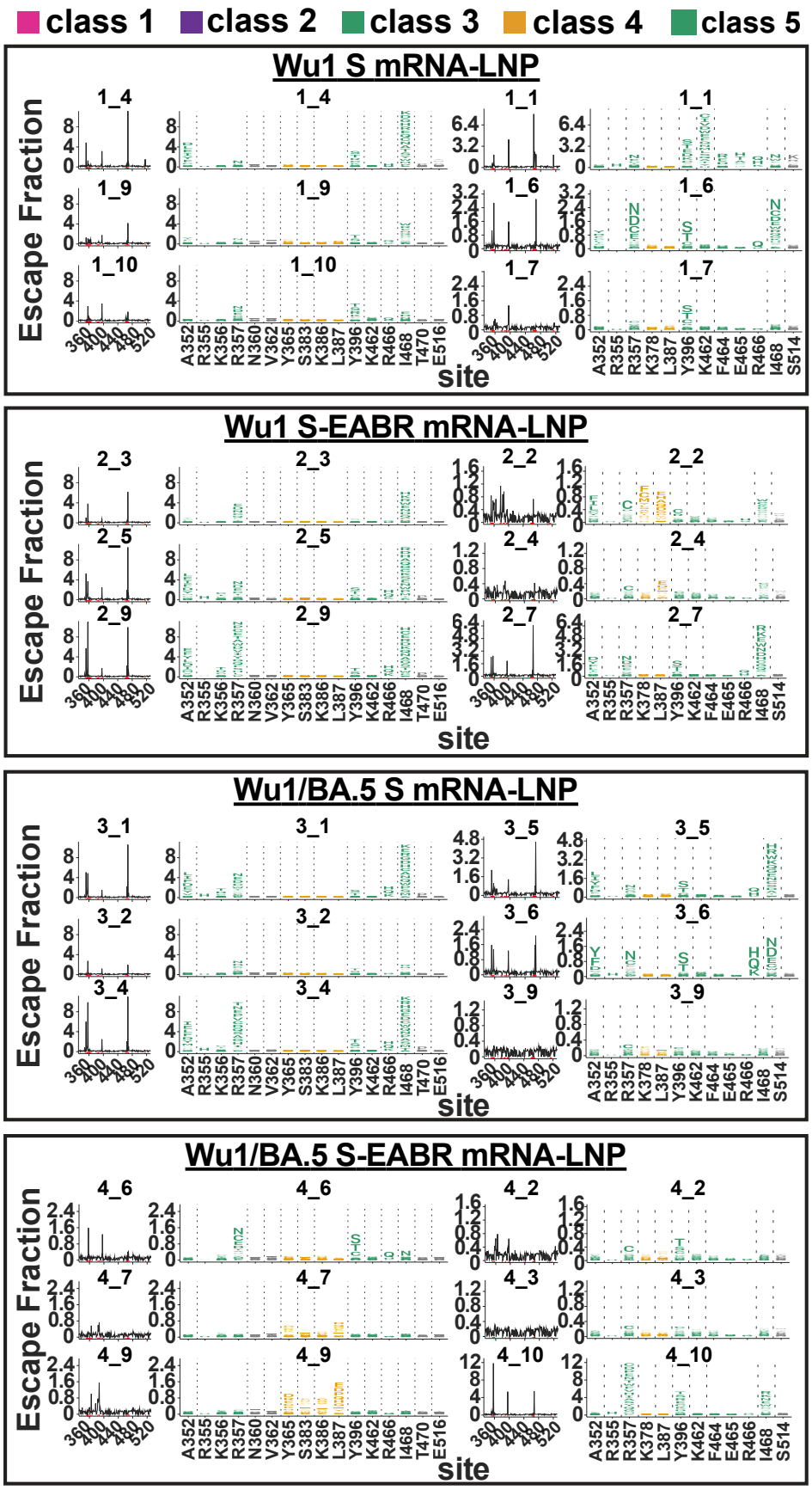
class 1
class 2
class 3
class 4
class 5
Wu1 S mRNA-LNP
Wu1 S-EABR mRNA-LNP
Wu1/BA.5 S mRNA-LNP
Wu1/BA.5 S-EABR mRNA-LNP
Escape Fraction
site

1010

1011 **Figure S8. Bivalent S-EABR mRNA-LNP booster induces less pronounced class 3**
1012 **Ab responses against XBB.1.5 RBD.** Sera for DMS studies were derived from pre-
1013 vaccinated mice that received booster immunizations with 2 μg of monovalent Wu1 S
1014 mRNA-LNP, monovalent Wu1 S-EABR mRNA-LNP, bivalent Wu1/BA.5 S mRNA-LNP, or
1015 bivalent Wu1/BA.5 S-EABR mRNA-LNP (immunization schedule in Fig. 1A-B). Line (left)
1016 and logo plots (right) are shown for DMS results for individual sera from pre-vaccinated
1017 mice that received the indicated boost immunogens. DMS was performed using an
1018 XBB.1.5 RBD library. The x axes of the line and logo plots display the RBD residue
1019 numbers. The y axis of the line plots shows the sum of the Ab escape of all mutations at
1020 a site (larger numbers indicating increased Ab escape). Sites with the strongest Ab
1021 escape are shown in logo plots, with tall letters representing the most frequent mutations
1022 at a site. Logo plots are colored differently for RBD epitopes within different
1023 classes[33,40] (epitopes are shown in Fig. S2; gray color for residues not assigned to an
1024 epitope).
1025

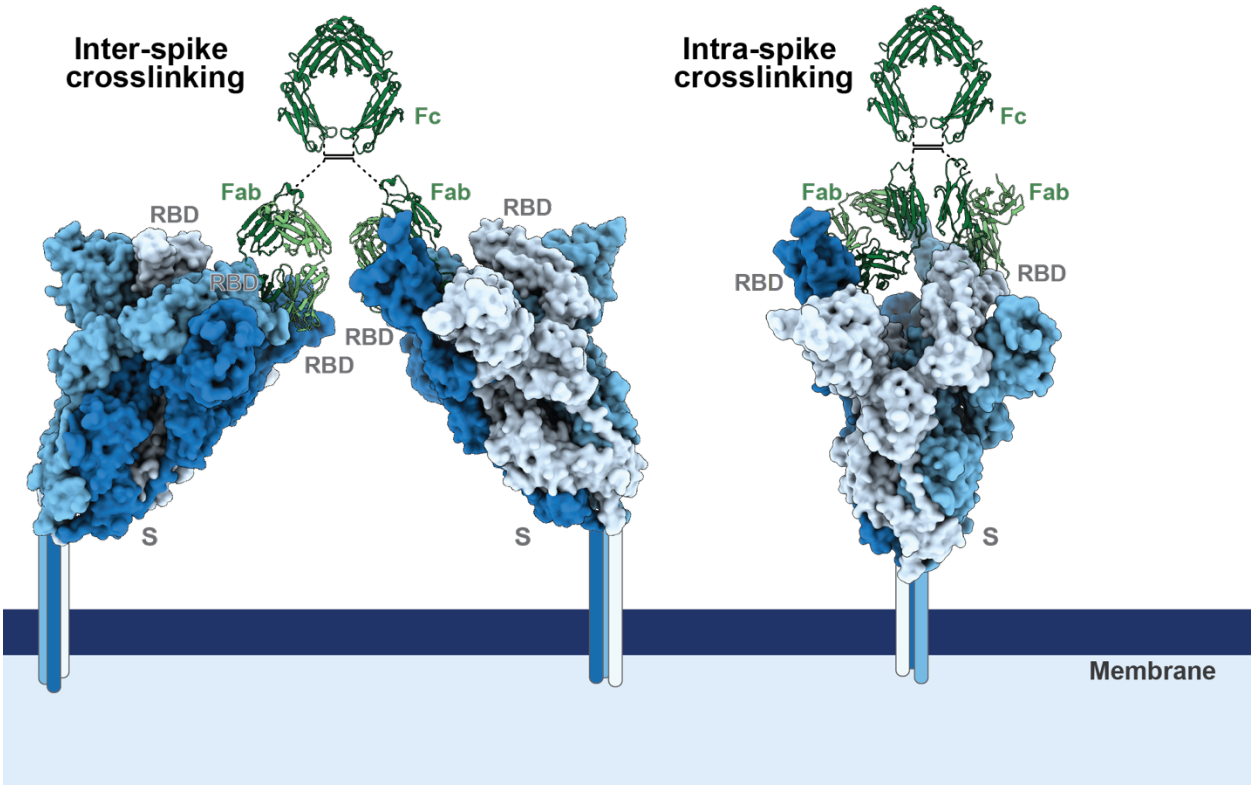

Figure S9. Cartoon diagram illustrating inter- and intra-S crosslinking. Left: model showing potential inter-S crosslinking through the interactions between both Fabs of a single IgG and two RBDs of adjacent viral S proteins. Right: model showing intra-S crosslinking through the interaction between both Fabs of a single IgG and two RBDs on the same viral S trimer. The hinge regions between the Fabs and Fc are modeled with flexible linkers, shown as dotted lines, as these regions were not resolved in the crystal structure of an intact IgG[76]. Disulfide bonds in the hinge region are shown as black lines. These diagrams are modeled based on the cryo-EM structure of SARS-CoV-2 S complexed with human C118 Fab (PDB ID 7RKV) and the crystal structure of human Fc (PDB ID 1FC1). IgGs shown in this figure represent either circulating Abs or membrane-bound BCRs.

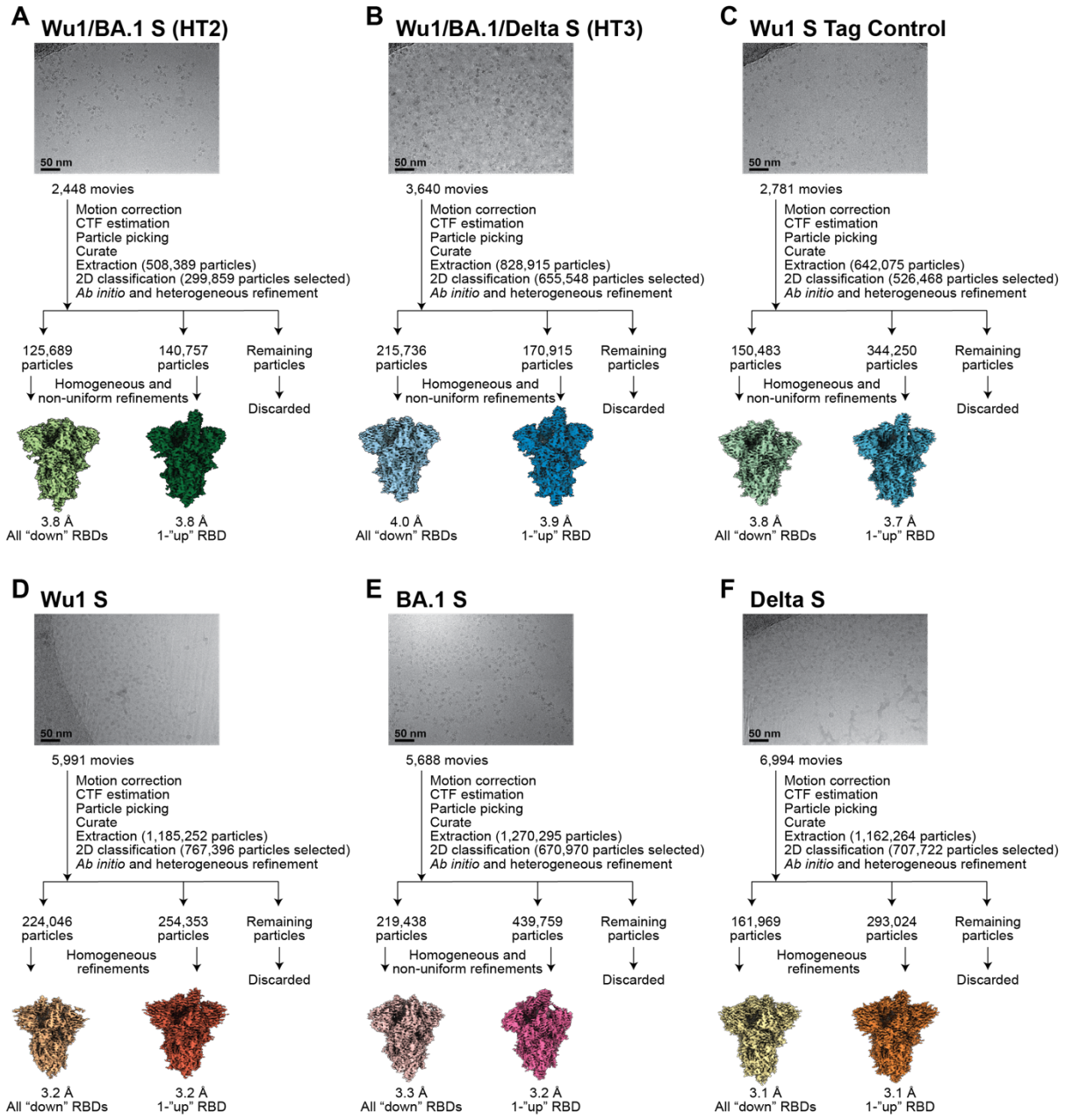

Figure S10. Cryo-EM data collection and processing for heterotrimeric and control SARS-CoV-2 S structures. Representative micrographs, workflow for single-particle data processing, and final reconstructions are shown for SARS-CoV-2 (**A**) Wu1/BA.1 S HT2 heterotrimer, (**B**) Wu1/BA.1/Delta S HT3 heterotrimer, and homotrimer S controls

1044 including (**C**) Wu1 His/StrepII double-tag control, (**D**) StrepII-tagged Wu1, (**E**) His-tagged

1045 BA.1, and (**F**) D7324-tagged Delta constructs.

1046

	Day 56				Day 154				Day 244			
	Wu1	**BA.5**	**BQ.1.1**	**XBB.1**	**Wu1**	**BA.5**	**BQ.1.1**	**XBB.1**	**Wu1**	**BA.5**	**BQ.1.1**	**XBB.1**
Cohort 1	56,855	274	58	50	17,843	136	50	50	74,875	851	69	75
Cohort 2	65,752	253	69	82	14,022	172	52	50	92,492	4,100	125	125
Cohort 3	60,300	513	74	57	14,130	159	50	50	80,978	4,441	169	108
Cohort 4	74,780	365	79	55	16,194	156	50	50	95,515	10,446	236	162

Table S1. Geometric mean neutralization titers. Day 56, 154, and 244 geometric mean neutralization titers for cohorts 1-4 against the Wu1, BA.5, BQ.1.1, and XBB.1 variants.

Boosting Immunogen	Animal	Wu1 DMS Profile	XBB.1.5 DMS Profile
Wu1 S mRNA-LNP	1_4	Moderate class 5 and 2	Strong class 5
Wu1 S mRNA-LNP	1_9		Strong class 5
Wu1 S mRNA-LNP	1_10	Moderate class 2	Strong class 5
Wu1 S mRNA-LNP	1_1	Moderate class 2	Strong class 5
Wu1 S mRNA-LNP	1_6	Polyclass	Strong class 5
Wu1 S mRNA-LNP	1_7	Polyclass	Moderate class 5
Wu1 S-EABR mRNA-LNP	2_3		Strong class 5
Wu1 S-EABR mRNA-LNP	2_5	Moderate class 2	Strong class 5
Wu1 S-EABR mRNA-LNP	2_9	Moderate class 2	Strong class 5
Wu1 S-EABR mRNA-LNP	2_2	Moderate class 2	Moderate class 5 and 4
Wu1 S-EABR mRNA-LNP	2_4	Polyclass	Polyclass
Wu1 S-EABR mRNA-LNP	2_7	Moderate class 2	Strong class 5
Wu1/BA.5 S mRNA-LNP	3_1	Moderate class 2	Strong class 5
Wu1/BA.5 S mRNA-LNP	3_2	Moderate class 1	Strong class 5
Wu1/BA.5 S mRNA-LNP	3_4	Strong class 2	Strong class 5
Wu1/BA.5 S mRNA-LNP	3_5	Polyclass	Strong class 5
Wu1/BA.5 S mRNA-LNP	3_6	Weak class 3	Strong class 5
Wu1/BA.5 S mRNA-LNP	3_9		Polyclass
Wu1/BA.5 S-EABR mRNA-LNP	4_6		Moderate class 5
Wu1/BA.5 S-EABR mRNA-LNP	4_7	Polyclass	Weak class 4
Wu1/BA.5 S-EABR mRNA-LNP	4_9	Polyclass	Moderate class 4
Wu1/BA.5 S-EABR mRNA-LNP	4_2	Polyclass	Weak class 5
Wu1/BA.5 S-EABR mRNA-LNP	4_3	Weak class 2	Polyclass
Wu1/BA.5 S-EABR mRNA-LNP	4_10	Polyclass	Strong class 5

	Escape fraction
Polyclass	<0.5
Weak	0.5-1
Moderate	1-2
Strong	>2

Table S2. Bivalent S-EABR mRNA-LNP booster induces consistent polyclass anti-RBD Ab responses. The DMS profiles for antisera from individual mice against the Wu1 and XBB.1.5 RBD libraries shown in Fig. S6 and S7 were classified as polyclass (total escape peaks <1 at all sites; green), moderate escape (total escape peaks between 1 and 2 at one or more sites; yellow), or strong escape (total escape peaks >2 at one or more sites; red) profiles. Total escape peaks represent the sum of escape fractions for all

1057 mutations at a specific site[45]. For moderate and strong escape profiles, the RBD epitope

1058 classes with the highest total escape peaks are specified.

1059 **References**

1060 1 Corbett, K. S. *et al.* SARS-CoV-2 mRNA vaccine design enabled by prototype pathogen
1061 preparedness. *Nature* **586**, 567-571 (2020). https://doi.org/10.1038/s41586-020-2622-0
1062 2 Zheng, C. *et al.* Real-world effectiveness of COVID-19 vaccines: a literature review and
1063 meta-analysis. *Int J Infect Dis* **114**, 252-260 (2022).
1064 https://doi.org/10.1016/j.ijid.2021.11.009
1065 3 Chen, Y. *et al.* Broadly neutralizing antibodies to SARS-CoV-2 and other human
1066 coronaviruses. *Nat Rev Immunol* **23**, 189-199 (2023). https://doi.org/10.1038/s41577-
1067 022-00784-3
1068 4 Hogan, M. J. & Pardi, N. mRNA Vaccines in the COVID-19 Pandemic and Beyond. *Annu*
1069 *Rev Med* **73**, 17-39 (2022). https://doi.org/10.1146/annurev-med-042420-112725
1070 5 Painter, M. M. *et al.* Rapid induction of antigen-specific CD4(+) T cells is associated with
1071 coordinated humoral and cellular immunity to SARS-CoV-2 mRNA vaccination. *Immunity*
1072 **54**, 2133-2142 e2133 (2021). https://doi.org/10.1016/j.immuni.2021.08.001
1073 6 Oberhardt, V. *et al.* Rapid and stable mobilization of CD8(+) T cells by SARS-CoV-2 mRNA
1074 vaccine. *Nature* **597**, 268-273 (2021). https://doi.org/10.1038/s41586-021-03841-4
1075 7 Polack, F. P. *et al.* Safety and Efficacy of the BNT162b2 mRNA Covid-19 Vaccine. *N Engl J*
1076 *Med* **383**, 2603-2615 (2020). https://doi.org/10.1056/NEJMoa2034577
1077 8 Baden, L. R. *et al.* Efficacy and Safety of the mRNA-1273 SARS-CoV-2 Vaccine. *N Engl J*
1078 *Med* **384**, 403-416 (2021). https://doi.org/10.1056/NEJMoa2035389
1079 9 Zhang, Z. *et al.* Humoral and cellular immune memory to four COVID-19 vaccines. *Cell*
1080 **185**, 2434-2451 e2417 (2022). https://doi.org/10.1016/j.cell.2022.05.022
1081 10 Planas, D. *et al.* Reduced sensitivity of SARS-CoV-2 variant Delta to antibody
1082 neutralization. *Nature* **596**, 276-280 (2021). https://doi.org/10.1038/s41586-021-03777-
1083 9
1084 11 Andrews, N. *et al.* Effectiveness of COVID-19 booster vaccines against COVID-19-related
1085 symptoms, hospitalization and death in England. *Nat Med* **28**, 831-837 (2022).
1086 https://doi.org/10.1038/s41591-022-01699-1
1087 12 WHO. Classification of Omicron (B.1.1.529): SARS-CoV-2 variant of concern., (2021).
1088 13 Liu, L. *et al.* Striking antibody evasion manifested by the Omicron variant of SARS-CoV-2.
1089 *Nature* **602**, 676-681 (2022). https://doi.org/10.1038/s41586-021-04388-0
1090 14 Cele, S. *et al.* Omicron extensively but incompletely escapes Pfizer BNT162b2
1091 neutralization. *Nature* **602**, 654-656 (2022). https://doi.org/10.1038/s41586-021-04387-
1092 1
1093 15 Andrews, N. *et al.* Covid-19 Vaccine Effectiveness against the Omicron (B.1.1.529)
1094 Variant. *N Engl J Med* **386**, 1532-1546 (2022). https://doi.org/10.1056/NEJMoa2119451
1095 16 Tseng, H. F. *et al.* Effectiveness of mRNA-1273 against SARS-CoV-2 Omicron and Delta
1096 variants. *Nat Med* **28**, 1063-1071 (2022). https://doi.org/10.1038/s41591-022-01753-y
1097 17 Gruell, H. *et al.* mRNA booster immunization elicits potent neutralizing serum activity
1098 against the SARS-CoV-2 Omicron variant. *Nat Med* **28**, 477-480 (2022).
1099 https://doi.org/10.1038/s41591-021-01676-0
1100 18 Wang, Q. *et al.* Alarming antibody evasion properties of rising SARS-CoV-2 BQ and XBB
1101 subvariants. *Cell* **186**, 279-286 e278 (2023). https://doi.org/10.1016/j.cell.2022.12.018

1102 19 Scheaffer, S. M. *et al.* Bivalent SARS-CoV-2 mRNA vaccines increase breadth of
1103 neutralization and protect against the BA.5 Omicron variant in mice. *Nat Med* **29**, 247-
1104 257 (2023). https://doi.org/10.1038/s41591-022-02092-8
1105 20 Khoury, D. S. *et al.* Predicting the efficacy of variant-modified COVID-19 vaccine boosters.
1106 *Nat Med* **29**, 574-578 (2023). https://doi.org/10.1038/s41591-023-02228-4
1107 21 Chalkias, S. *et al.* A Bivalent Omicron-Containing Booster Vaccine against Covid-19. *N*
1108 *Engl J Med* **387**, 1279-1291 (2022). https://doi.org/10.1056/NEJMoa2208343
1109 22 Collier, A. Y. *et al.* Immunogenicity of BA.5 Bivalent mRNA Vaccine Boosters. *N Engl J Med*
1110 **388**, 565-567 (2023). https://doi.org/10.1056/NEJMc2213948
1111 23 Davis-Gardner, M. E. *et al.* Neutralization against BA.2.75.2, BQ.1.1, and XBB from mRNA
1112 Bivalent Booster. *N Engl J Med* **388**, 183-185 (2023).
1113 https://doi.org/10.1056/NEJMc2214293
1114 24 Wang, Q. *et al.* Deep immunological imprinting due to the ancestral spike in the current
1115 bivalent COVID-19 vaccine. *Cell Rep Med* **4**, 101258 (2023).
1116 https://doi.org/10.1016/j.xcrm.2023.101258
1117 25 Wang, Q. *et al.* SARS-CoV-2 neutralising antibodies after bivalent versus monovalent
1118 booster. *Lancet Infect Dis* **23**, 527-528 (2023). https://doi.org/10.1016/S1473-
1119 3099(23)00181-0
1120 26 Alsoussi, W. B. *et al.* SARS-CoV-2 Omicron boosting induces de novo B cell response in
1121 humans. *Nature* **617**, 592-598 (2023). https://doi.org/10.1038/s41586-023-06025-4
1122 27 Park, Y. J. *et al.* Imprinted antibody responses against SARS-CoV-2 Omicron sublineages.
1123 *Science* **378**, 619-627 (2022). https://doi.org/10.1126/science.adc9127
1124 28 Carreno, J. M., Singh, G., Simon, V., Krammer, F. & group, P. V. I. s. Bivalent COVID-19
1125 booster vaccines and the absence of BA.5-specific antibodies. *Lancet Microbe* **4**, e569
1126 (2023). https://doi.org/10.1016/S2666-5247(23)00118-0
1127 29 Cobey, S. & Hensley, S. E. Immune history and influenza virus susceptibility. *Curr Opin*
1128 *Virol* **22**, 105-111 (2017). https://doi.org/10.1016/j.coviro.2016.12.004
1129 30 Song, S. *et al.* A systematic review and meta-analysis on the effectiveness of bivalent
1130 mRNA booster vaccines against Omicron variants. *Vaccine* **42**, 3389-3396 (2024).
1131 https://doi.org/10.1016/j.vaccine.2024.04.049
1132 31 Hoffmann, M. A. G. *et al.* ESCRT recruitment to SARS-CoV-2 spike induces virus-like
1133 particles that improve mRNA vaccines. *Cell* (2023).
1134 https://doi.org/https://doi.org/10.1016/j.cell.2023.04.024
1135 32 Hsieh, C. L. *et al.* Structure-based design of prefusion-stabilized SARS-CoV-2 spikes.
1136 *Science* **369**, 1501-1505 (2020). https://doi.org/10.1126/science.abd0826
1137 33 Barnes, C. O. *et al.* SARS-CoV-2 neutralizing antibody structures inform therapeutic
1138 strategies. *Nature* **588**, 682-687 (2020). https://doi.org/10.1038/s41586-020-2852-1
1139 34 Li, C. J. & Chang, S. C. SARS-CoV-2 spike S2-specific neutralizing antibodies. *Emerg*
1140 *Microbes Infect* **12**, 2220582 (2023). https://doi.org/10.1080/22221751.2023.2220582
1141 35 Crawford, K. H. D. *et al.* Protocol and Reagents for Pseudotyping Lentiviral Particles with
1142 SARS-CoV-2 Spike Protein for Neutralization Assays. *Viruses* **12** (2020).
1143 https://doi.org/10.3390/v12050513
1144 36 Robbiani, D. F. *et al.* Convergent antibody responses to SARS-CoV-2 in convalescent
1145 individuals. *Nature* **584**, 437-442 (2020). https://doi.org/10.1038/s41586-020-2456-9

37 Wang, Z. *et al.* Analysis of memory B cells identifies conserved neutralizing epitopes on the N-terminal domain of variant SARS-Cov-2 spike proteins. *Immunity* **55**, 998-1012 e1018 (2022). https://doi.org/10.1016/j.immuni.2022.04.003

38 Miller, J. *et al.* Substantial Neutralization Escape by SARS-CoV-2 Omicron Variants BQ.1.1 and XBB.1. *N Engl J Med* **388**, 662-664 (2023). https://doi.org/10.1056/NEJMc2214314

39 Feng, S. *et al.* Correlates of protection against symptomatic and asymptomatic SARS-CoV-2 infection. *Nat Med* **27**, 2032-2040 (2021). https://doi.org/10.1038/s41591-021-01540-1

40 Fan, C. *et al.* Neutralizing monoclonal antibodies elicited by mosaic RBD nanoparticles bind conserved sarbecovirus epitopes. *Immunity* **55**, 2419-2435 e2410 (2022). https://doi.org/10.1016/j.immuni.2022.10.019

41 Fan, C. *et al.* Cross-reactive sarbecovirus antibodies induced by mosaic RBD nanoparticles. *Proc Natl Acad Sci U S A* **122**, e2501637122 (2025). https://doi.org/10.1073/pnas.2501637122

42 Starr, T. N. *et al.* Deep Mutational Scanning of SARS-CoV-2 Receptor Binding Domain Reveals Constraints on Folding and ACE2 Binding. *Cell* **182**, 1295-1310 e1220 (2020). https://doi.org/10.1016/j.cell.2020.08.012

43 Taylor, A. L. & Starr, T. N. Deep mutational scans of XBB.1.5 and BQ.1.1 reveal ongoing epistatic drift during SARS-CoV-2 evolution. *PLoS Pathog* **19**, e1011901 (2023). https://doi.org/10.1371/journal.ppat.1011901

44 Cohen, A. A. *et al.* Mosaic sarbecovirus nanoparticles elicit cross-reactive responses in pre-vaccinated animals. *Cell* **187**, 5554-5571 e5519 (2024). https://doi.org/10.1016/j.cell.2024.07.052

45 Greaney, A. J. *et al.* Mapping mutations to the SARS-CoV-2 RBD that escape binding by different classes of antibodies. *Nat Commun* **12**, 4196 (2021). https://doi.org/10.1038/s41467-021-24435-8

46 Callaway, H. M. *et al.* Bivalent intra-spike binding provides durability against emergent Omicron lineages: Results from a global consortium. *Cell Rep* **42**, 112014 (2023). https://doi.org/10.1016/j.celrep.2023.112014

47 Sanders, R. W. *et al.* A next-generation cleaved, soluble HIV-1 Env trimer, BG505 SOSIP.664 gp140, expresses multiple epitopes for broadly neutralizing but not non-neutralizing antibodies. *PLoS Pathog* **9**, e1003618 (2013). https://doi.org/10.1371/journal.ppat.1003618

48 Walls, A. C. *et al.* Structure, Function, and Antigenicity of the SARS-CoV-2 Spike Glycoprotein. *Cell* **181**, 281-292 e286 (2020). https://doi.org/10.1016/j.cell.2020.02.058

49 Wrapp, D. *et al.* Cryo-EM structure of the 2019-nCoV spike in the prefusion conformation. *Science* **367**, 1260-1263 (2020). https://doi.org/10.1126/science.abb2507

50 Tan, C. Y. *et al.* Effectiveness of bivalent mRNA vaccines against medically attended symptomatic SARS-CoV-2 infection and COVID-19-related hospital admission among SARS-CoV-2-naive and previously infected individuals: a retrospective cohort study. *Lancet Infect Dis* **23**, 1343-1348 (2023). https://doi.org/10.1016/S1473-3099(23)00373-0

51 Bowen, J. E. *et al.* SARS-CoV-2 spike conformation determines plasma neutralizing activity elicited by a wide panel of human vaccines. *Sci Immunol* **7**, eadf1421 (2022). https://doi.org/10.1126/sciimmunol.adf1421

1190 52 Balinsky, C. A. *et al.* Antibodies to S2 domain of SARS-CoV-2 spike protein in Moderna
1191 mRNA vaccinated subjects sustain antibody-dependent NK cell-mediated cell cytotoxicity
1192 against Omicron BA.1. *Front Immunol* **14**, 1266829 (2023).
1193 https://doi.org/10.3389/fimmu.2023.1266829
1194 53 Keeton, R. *et al.* T cell responses to SARS-CoV-2 spike cross-recognize Omicron. *Nature*
1195 **603**, 488-492 (2022). https://doi.org/10.1038/s41586-022-04460-3
1196 54 Rydyznski Moderbacher, C. *et al.* Antigen-Specific Adaptive Immunity to SARS-CoV-2 in
1197 Acute COVID-19 and Associations with Age and Disease Severity. *Cell* **183**, 996-1012
1198 e1019 (2020). https://doi.org/10.1016/j.cell.2020.09.038
1199 55 Muik, A. *et al.* Exposure to BA.4/5 S protein drives neutralization of Omicron BA.1, BA.2,
1200 BA.2.12.1, and BA.4/5 in vaccine-experienced humans and mice. *Sci Immunol* **7**,
1201 eade9888 (2022). https://doi.org/10.1126/sciimmunol.ade9888
1202 56 Ying, B. *et al.* Boosting with variant-matched or historical mRNA vaccines protects
1203 against Omicron infection in mice. *Cell* **185**, 1572-1587 e1511 (2022).
1204 https://doi.org/10.1016/j.cell.2022.03.037
1205 57 Pallesen, J. *et al.* Immunogenicity and structures of a rationally designed prefusion
1206 MERS-CoV spike antigen. *Proc Natl Acad Sci U S A* **114**, E7348-E7357 (2017).
1207 https://doi.org/10.1073/pnas.1707304114
1208 58 McBride, C. E., Li, J. & Machamer, C. E. The cytoplasmic tail of the severe acute
1209 respiratory syndrome coronavirus spike protein contains a novel endoplasmic reticulum
1210 retrieval signal that binds COPI and promotes interaction with membrane protein. *J Virol*
1211 **81**, 2418-2428 (2007). https://doi.org/10.1128/JVI.02146-06
1212 59 Korber, B. *et al.* Tracking Changes in SARS-CoV-2 Spike: Evidence that D614G Increases
1213 Infectivity of the COVID-19 Virus. *Cell* **182**, 812-827 e819 (2020).
1214 https://doi.org/10.1016/j.cell.2020.06.043
1215 60 Miettinen, H. M., Rose, J. K. & Mellman, I. Fc receptor isoforms exhibit distinct abilities
1216 for coated pit localization as a result of cytoplasmic domain heterogeneity. *Cell* **58**, 317-
1217 327 (1989). https://doi.org/10.1016/0092-8674(89)90846-5
1218 61 Pinto, D. *et al.* Broad betacoronavirus neutralization by a stem helix-specific human
1219 antibody. *Science* (2021). https://doi.org/10.1126/science.abj3321
1220 62 Kariko, K. *et al.* Incorporation of pseudouridine into mRNA yields superior
1221 nonimmunogenic vector with increased translational capacity and biological stability.
1222 *Mol Ther* **16**, 1833-1840 (2008). https://doi.org/10.1038/mt.2008.200
1223 63 Kariko, K., Muramatsu, H., Ludwig, J. & Weissman, D. Generating the optimal mRNA for
1224 therapy: HPLC purification eliminates immune activation and improves translation of
1225 nucleoside-modified, protein-encoding mRNA. *Nucleic Acids Res* **39**, e142 (2011).
1226 https://doi.org/10.1093/nar/gkr695
1227 64 Pardi, N. *et al.* Expression kinetics of nucleoside-modified mRNA delivered in lipid
1228 nanoparticles to mice by various routes. *J Control Release* **217**, 345-351 (2015).
1229 https://doi.org/10.1016/j.jconrel.2015.08.007
1230 65 Hsieh, C. L. *et al.* Prefusion-stabilized SARS-CoV-2 S2-only antigen provides protection
1231 against SARS-CoV-2 challenge. *Nat Commun* **15**, 1553 (2024).
1232 https://doi.org/10.1038/s41467-024-45404-x

66 Cohen, A. A. *et al.* Mosaic RBD nanoparticles protect against challenge by diverse sarbecoviruses in animal models. *Science* **377**, eabq0839 (2022). https://doi.org/10.1126/science.abq0839

67 Mastronarde, D. N. Automated electron microscope tomography using robust prediction of specimen movements. *J Struct Biol* **152**, 36-51 (2005). https://doi.org/10.1016/j.jsb.2005.07.007

68 Punjani, A., Rubinstein, J. L., Fleet, D. J. & Brubaker, M. A. cryoSPARC: algorithms for rapid unsupervised cryo-EM structure determination. *Nat Methods* **14**, 290-296 (2017). https://doi.org/10.1038/nmeth.4169

69 Cohen, A. A. *et al.* Mosaic nanoparticles elicit cross-reactive immune responses to zoonotic coronaviruses in mice. *Science* **371**, 735-741 (2021). https://doi.org/10.1126/science.abf6840

70 West, A. P., Jr. *et al.* Computational analysis of anti-HIV-1 antibody neutralization panel data to identify potential functional epitope residues. *Proc Natl Acad Sci U S A* **110**, 10598-10603 (2013). https://doi.org/10.1073/pnas.1309215110

71 Starr, T. N. *et al.* Shifting mutational constraints in the SARS-CoV-2 receptor-binding domain during viral evolution. *Science* **377**, 420-424 (2022). https://doi.org/10.1126/science.abo7896

72 Greaney, A. J. *et al.* Comprehensive mapping of mutations in the SARS-CoV-2 receptor-binding domain that affect recognition by polyclonal human plasma antibodies. *Cell Host Microbe* **29**, 463-476 e466 (2021). https://doi.org/10.1016/j.chom.2021.02.003

73 Hills, R. A. *et al.* Proactive vaccination using multiviral Quartet Nanocages to elicit broad anti-coronavirus responses. *Nat Nanotechnol* **19**, 1216-1223 (2024). https://doi.org/10.1038/s41565-024-01655-9

74 Barnes, C. O. *et al.* SARS-CoV-2 neutralizing antibody structures inform therapeutic strategies. *Nature* **588**, 682-687 (2020). https://doi.org/10.1038/s41586-020-2852-1

75 Landau, M. *et al.* ConSurf 2005: the projection of evolutionary conservation scores of residues on protein structures. *Nucleic Acids Res* **33**, W299-302 (2005). https://doi.org/10.1093/nar/gki370

76 Saphire, E. O. *et al.* Crystal structure of a neutralizing human IGG against HIV-1: a template for vaccine design. *Science* **293**, 1155-1159 (2001).

Acknowledgements

We thank J. Vielmetter, A. Lam, and the Caltech Protein Expression Center for assistance with protein production, S. Chen and the Caltech Cryo-EM facility for cryo-EM data collection, M. Anaya (Caltech) for a BirA expression plasmid, J.E. Robinson (Tulane University) for the JR-52 antibody, J. Bloom (Fred Hutchinson Cancer Research Center) and T. Starr (University of Utah) for RBD libraries, and J. Bloom (Fred Hutchinson) and P.

Bieniasz (Rockefeller University) for neutralization assay reagents. We thank J. Keeffe for guidance on ELISA method development, A. West for Swift DMS support, Y. Tam (Acuitas Therapeutics) for careful reading of the manuscript, B. Wold, G. Tolomiczenko, and the Caltech Merkin Institute for Translational Research for helpful discussions. Cryo-EM was performed in the Beckman Institute Resource Center for Transmission Electron Microscopy at Caltech. We thank Labcorp Drug Development–Antibody Reagents and Vaccines (Denver, PA) (formerly Covance, Inc.) for mouse immunization studies, and RNAcore (Houston Methodist Research Institute) for synthesis of mRNAs and helpful discussion. Figures 1A, 1C, and 5A were created with Biorender.com. These studies were funded by Wellcome Leap (P.J.B.), the National Institutes of Health P01-AI165075 (P.J.B.) and DP5OD033362 (M.A.G.H), Gates Foundation INV-034638 (P.J.B.) and INV-056219 (M.A.G.H.), the Merkin Institute for Translational Research (Caltech) (P.J.B), and the George Mason University Fast Grants (P.J.B.). This manuscript is the result of funding in whole or in part by the National Institutes of Health (NIH). It is subject to the NIH Public Access Policy. Through acceptance of this federal funding, NIH has been given a right to make this manuscript publicly available in PubMed Central upon the Official Date of Publication, as defined by NIH.

Author contributions:

Conceptualization: C.F., A.A.C., K.A.D., P.J.B., and M.A.G.H.; Methodology: C.F., A.A.C., K.A.D., A.-C.P.F., P.J.B., and M.A.G.H.; Investigation: C.F., A.A.C., K.A.D., A.V.R., A.-C.P.F., Z.Y., P.N.P.G., K.E.H.T., W.J.M., P.J.C.L., and M.A.G.H.; Writing – original draft: C.F., A.A.C., K.A.D., P.J.B., and M.A.G.H.; Writing – review and editing: C.F., A.A.C.,

K.A.D., A.-C.P.F., P.J.C.L., P.J.B., and M.A.G.H.; Visualization: C.F., A.A.C., K.A.D.; Supervision: P.J.B., and M.A.G.H.; Funding: P.J.B., and M.A.G.H.

Competing interests

M.A.G.H. and P.J.B. are inventors on a US patent application filed by the California Institute of Technology that covers the EABR technology described in this work. P.J.B. is a scientific advisor for Vaccine Company, Inc. M.A.G.H. is a scientific consultant for Vaccine Company, Inc. W.J.M. and P.J.C.L. are employees of Acuitas Therapeutics, a company developing lipid nanoparticle delivery technology; P.J.C.L. holds equity in Acuitas Therapeutics.

Materials, data, and code availability

Materials generated in this study are available upon request through a Materials Transfer Agreement. Code used for data processing and visualization of DMS results is available upon request. Main text and supplementary data will be publicly available. DMS raw sequencing data will be available under an NCBI SRA. Cryo-EM density maps are deposited in the EMDB with accession codes: EMD-71513, EMD-71514, EMD-71515 and EMD-71516. Materials are available upon request to corresponding authors with a signed material transfer agreement, and other information required to analyze the data in this paper is available from the lead contacts upon request. This paper does not report original code. The work is licensed under a Creative Commons Attribution 4.0 International (CC BY 4.0) license, which permits unrestricted use, distribution, and reproduction in any medium, provided the original work is properly cited. To view a copy of this license, visit

https://creativecommons.org/licenses/by/4.0/. This license does not apply to figures/photos/artwork or other content included in the article that is credited to a third party; obtain authorization from the rights holder before using such material.